Nonlinear dynamic analysis of solution multiplicity of buoyancy ventilation in a typical underground structure

Yanan Liu[a,b], Yimin Xiao[a,c*], Jianli Chen[d],

[a] School of Civil Engineering, Chongqing University, Chongqing 400045, China

[b] Key Laboratory of New Technology for Construction of Cities in Mountain Area of Ministry of Education, Chongqing University, Chongqing 400045, China

[c] National Centre for International Research of Low-carbon and Green Buildings, Chongqing University, Chongqing 400045, China

[d] National Renewable Energy Lab, USA

*Corresponding email: xiaoyimin@cqu.edu.cn

Postal address: School of Civil Engineering, Chongqing University, Chongqing, 400045, China

Abstract:

Buoyancy ventilation is widely used in underground buildings, such as underground hydropower stations. Multiple solutions of buoyancy ventilation may exist in those underground structures. In this study, we developed a transient model comprising an ordinary differential equation system to describe buoyancy ventilation patterns in typical two-zone underground structures. Additionally, the accuracy of the model was validated. Nonlinear dynamical analysis was conducted to study multiple steady-state airflow. According to mathematical derivation, the configuration of one local heat source at the bottom corner introduces two stable solutions. The criterion to determine the stability and existence of solutions for more general scenarios was developed. Using this criterion, we obtained the multiple steady states of any two-zone underground buildings for different stack height ratios and the strength ratios of the heat sources.

This criterion can be adopted for the design of buoyancy ventilation or natural smoke ventilation systems. Designers can change the height ratio of the stack or the heat ratio of two zones to induce the desired ventilation patterns. Finally, a case study was conducted with field measurements to demonstrate the use of the nonlinear dynamical analysis method to investigate the multiple steady states of buoyancy ventilation. Through the case study, we validated that the proposed criterion could produce the same result as the nonlinear dynamical analysis.

Keywords： Nonlinear dynamics; buoyancy ventilation; multiple steady states；Underground buildings

Nomenclature

A_1	Coefficient matrix for linearized differential equation system
q_1	Mass flow rate at zone 1, [kg/s]
q_2	Mass flow rate at zone 2, [kg/s]
T_1	Air temperature at zone 1, [K]
T_a	Outdoor air temperature, [K]
S_1	Coefficient of Mass flow impedance at zone1
S_2	Coefficient of Mass flow impedance at zone2
M_1	Thermal mass at zone 1, [kg]
M_2	Thermal mass at zone 2, [kg]
E_1	Total heat gain at zone 1 , [kW]
E_2	Total heat gain at zone 2 , [kW]
C_p	Specific heat of air,[kJ/(kg·K)]
t	Time, [s]
g	Gravitational acceleration, [m/s^2]
H_1	Height of zone 1,[m]
H_2	Height of zone 2,[m]
κ	Heat ratio between two zones, $\frac{E_2}{E_1}$

ΔT_1	Temperature difference between indoor and outdoor air at zone 1, [℃]
ΔT_2	Temperature difference between indoor and outdoor air at zone 2, [℃]
α	Height ratio between two zones, $\frac{H_2}{H_1}$
$\overline{\Delta T_1}$	Temperature difference between indoor and outdoor air at zone 1 in steady state, [℃]
$\overline{\Delta T_2}$	Temperature difference between indoor and outdoor air at zone 1 in steady state, [℃]
ρ_0	Ambient air density, [kg/m^3]
λ	Eigenvalue of coefficient matrix

1. Introduction

Owing to the wide utilization of underground spaces, the evaluation of natural ventilation in underground buildings has become significant [1-11]. Natural ventilation as a passive strategy has been adopted in many underground structures, such as underground shelters [1], warehouses [2],underground garages [3, 4], mines [5], hydropower stations [8, 9], and underground roads and railway tunnels [10]. Aspects such as air quality [3, 4], energy conservations [6, 7], computational models [5, 8, 9], fire safety [5, 10], and ventilation performance [1, 2] have been investigated. Hence, as a type of natural ventilation, buoyancy ventilation in underground structures is worth investigating.

Buoyancy ventilation is the air flow driven by the air density difference caused by air temperature difference. As early as 1954, Batchelor [12] began investigating the buoyancy of airflow. Many factors, such as envelope heat transfer or internal heat source, can result in thermal ventilation. Among them, various studies have been performed regarding solar-chimney-induced thermal ventilation [13, 14], natural ventilation reinforced by double-skin facade [15-20], indoor thermal plume, and single-

sided [21] or cross ventilation [22, 23] driven by the separate or combined effect of buoyancy and wind pressure.

For the ventilation driven by the combined effect of buoyancy and wind pressure, multiple solutions may exist. Hunt G.R & Linden.P.F [24] first raised the issue of mutual reinforcement and confrontation of natural ventilation under wind pressure and thermal pressure. However, they primarily studied the situation with the reinforced effect of wind pressure and thermal pressure. A one-dimensional mathematical model was proposed with a visual and quantitative comparative study performed using a small-scaled brine model experiment. This study provides a theoretical basis and guide for the calculation of natural ventilation of night cooling or air purging system of gas leakage. As the first study that introduced the (concept or possibility) of multiple solutions of building ventilation and smoke exhaust, Nitta [25] demonstrated that solution multiplicity exists under specific room layouts and fan settings in the design of smoke prevention and exhaust. This study presents the importance of solution multiplicity to personnel safety and ventilation design, although its formation mechanism is not elaborated.

Subsequently, the solution multiplicity of single-zone and double-opening buildings under the combined effect of wind pressure and thermal pressure has attracted wide attention. The existence of solution multiplicity was first investigated, where multiple methods were employed to reproduce this phenomenon. Heiselberg et al. [26] analyzed the multiple steady sates of the single-zone and double-opening buildings with wind pressure and buoyancy confrontation by a salt water experiment and CFD simulation. Based on this typical building configuration, Li & Delsante [27] established a complete one-dimensional mathematical model while considering the effect of heat transfer in the building envelope. Additionally, Li [28] reported that solution multiplicity could exist in both inclined tunnels and two-story aboveground buildings, although the focus of the study was wind pressure and buoyancy confrontation in a single-zone building. Subsequently, the dynamical process and impact factors of multiple steady states were

investigated. Lishman & Woods [29] studied the effect of wind pressure changes on the transition of multiple steady states in a single-zone building. Yuan & Glicksman [30-32] studied the effects of different initial conditions on the formation of multiple steady states in single-zone buildings under the combined effect of wind pressure and buoyancy. The dynamic transition between different steady states was investigated considering the effects of disturbance magnitude and action time. Gladstone et al. [33] studied a single-zone building with distributed heat sources on the floor. The effects of distributed roof cold source, outdoor temperature gradient, and outdoor wind pressure on multiple steady states were discussed. In the study, they proposed a one-dimensional model and compared it with experiments. Erhan & Hifzi [34] used IEA Annex 20 as an example and discovered that different turbulence parameters may produce multiple solutions in CFD simulations.

In addition, other studies focusing on the solution multiplicity of ventilation in single-zone and multiopening buildings have been performed. Chenvidakarn & Woods [35] and Durrani et al. [36] analyzed the solution multiplicity of a typical aboveground building through a saltwater experiment employing one-dimensional model analyses [35] and CFD simulations [36].The building contained one zone and three openings. Two upper openings were the chimneys, while a lower large opening was the entrance door. However, these studies primarily focused on the accuracy comparison of the LES model with K-e model in CFD. The analytical model was established based on an equilibrium state without considering the effect of thermal mass and time; therefore, an in-depth analysis of the stability of multiple solutions was not performed. Chen & Li [37] studied the buoyancy ventilation of a single-zone building with three horizontal openings in different levels using theoretical analysis. For a specific geometric structure, even with the same boundary conditions and geometric settings, the height of thermal stratification might be higher or lower than the medium-level horizontal opening when the initial conditions are different.

In a fire, the solution multiplicity of smoke flows is a significant topic that can guide

the design of smoke exhaust systems, thereby ensuring the safety of human evacuation. Gong J. and Li Y. [38, 39] studied the solution multiplicity of smoke spread with the effect of outdoor wind pressure in fires. The research involved both small-scaled experiments and CFD simulations, including a single heat source in a typical single-zone building and a single heat source in a two-zone building. A comparative study was conducted using different forms of heat sources, such as point, line, and area heat sources. In the study, they investigated the effects of different heat source locations on solution multiplicity and presented a visualization experiment. Yang D. [40] analyzed the confrontation between outdoor wind pressure and thermal pressure caused by fire in an oblique straight tunnel. The one-dimensional model, which was based on the transient energy balance and pressure balance of a single-zone building to establish a nonlinear differential equation, was similar to that of Yuan & Glicksman [31], despite the difference in geometry. Furthermore, the application scenario of the study was different, in that it was suitable for the fire situation in the oblique straight tunnel instead of a single-zone building. Furthermore, salt water experiments were conducted to compare the entire process of formation and development of the two steady-state solutions.

Additionally, studies regarding the solution multiplicity of ventilation in two-zone spaces have been performed. Yang L. [41, 42] performed a detailed analysis of multiple steady states and bifurcation of fluids in a two-zone building with four openings using theoretical analyses and CFD simulations. Li [43] et al. investigated the buoyancy ventilation in a two-story space with two heat sources and three openings. A mathematical model was established using the nonlinear ordinary differential equation. The effect of the heat source's strength ratio on fluid bifurcation was analyzed. Yang D. [44] analyzed the smoke exhaust spread in a tunnel with three entrances in fire scenarios and concluded that six equilibrium states might exist. Subsequently, based on the energy balance and pressure balance equations of the steady states, a mathematical model was established to solve the smoke exhaust of each tunnel. CFD was also used to simulate

and reproduce some of the steady states. However, in the proposed one-dimensional model that was based on equilibrium conditions, the transient development process of smoke ventilation was not considered. Additionally, the stability of the solution was not analyzed. Liu et al. [45] numerically studied the formation process of multiple steady states in an underground building with two tunnel connecting to the outdoor environment. The tunnels were set with equal heights with only one heat source at the corner of the deep buried spaces. The authors used the two-stage CFD method to reproduce the two steady states of the buoyancy ventilation in the underground building by changing the initial conditions. This study primarily provided a method to investigate the multiple steady states.

In summary, despite the abovementioned studies, gaps still exist in predicting and analyzing the multiplicity of buoyancy ventilation in underground buildings. First, current studies are still limited to scenarios with single zones or two zones driven by combined wind and buoyancy. More specifically, the building configurations and driving forces are different. For the building configurations, most studies focus on single-zone buildings with two openings, which differ from underground structures. Typically, at least two tunnels are connected with the outdoor environment. Hence, at least two zones exist for the underground structures provided that the height of the deep buried rooms are neglected. For the driven forces, the combat between thermal buoyancy and wind pressure is the main cause of solution multiplicity in previous studies. However, underground buildings are not exposed to the outdoor environment, and the wind pressure is not highly significant. By contrast, the heat transfer between the indoor air and surrounding soil can affect the thermal pressure inside the tunnel. Therefore, both zones may need to be considered as heat sources/sinks. The charge and discharge process of heat from the soil to the tunnel can contribute to the solution multiplicity of buoyancy ventilation in underground buildings. Additionally, heat is released from the indoor environment, such as from equipment and human body; therefore, the solution multiplicity of natural ventilation is driven by the combat of

thermal pressure between two tunnels. Next, the current studies are not generalizable. To study multiple steady states, the CFD method or analytical method must be repeated each time the geometry is changed. Especially for the CFD method, the initial conditions must be changed and numerous CFD simulations must be conducted to study the existence of multiple steady states for a single fixed geometry. This requires significant computational resources and manpower. For the analytical method, the strength of the buoyancy and the wind pressure are the main control parameters studied to investigate solution multiplicity. In other words, buoyancy and wind pressure were altered to investigate their effects on the performances of multiple steady states. This may be useful for aboveground buildings if the geometry is fixed. However, for a more general case, the height ratio of the tunnel may be an important control parameter.

In our study, we considered both the effects of the strength ratio of heat sources and the different height ratios of tunnels simultaneously. To attain a deep understanding of the solution multiplicity of underground buoyancy ventilation, we performed a nonlinear dynamical analysis to study the formation mechanism of multiple steady states. In addition to demonstrating the use of nonlinear dynamics to analyze the buoyancy ventilation in underground buildings, our goal is to develop a criterion for evaluating the multiple steady states for different buildings and heat source configurations. This criterion is based on the strength ratio of the heat sources between two zones and the tunnel height ratio of two zones. Once these two parameters are determined, then whether a solution multiplicity exists for a typical underground structure with two tunnels connected to the outdoor environment can be determined. This is a straightforward method for the design and optimization of buoyancy ventilation and smoke ventilation in underground buildings.

The organization of this paper is as follows: Section 1 presents the literature review of previous studies regarding buoyancy ventilation and solution multiplicity with an emphasis on the significance of our study; Section 2 provides the nonlinear dynamic analysis of a typical underground structure, which includes the establishment of a one-

dimensional model, stability and existence analysis of underground buoyancy ventilation, model validation through result comparison with previous literature, and graphical presentation of multiple steady states through bifurcation diagram and phase portrait; Section 3 presents a case study of an underground hydropower station to demonstrate how nonlinear dynamical analysis is employed in real project applications. Furthermore, the derived criterion is compared with the analysis results; Section 4 presents the conclusions, and current studies are summarized along with future studies.

2. Nonlinear dynamic analysis

To study the nonlinear dynamics of typical deep-buried underground buildings with two openings, we first established the transient mathematical mode. Some assumptions were made: (1) Each zone was well mixed;（2）Thermal mass was 1;（3）$E_1 > 0$; (4) The mass flow impedance coefficient of the geometry was constant. The conservation law was adopted to develop the transient model. As the driven force of the ventilation is the thermal pressure in two tunnels, as illustrated in Fig. 1, we divided the building into two zones. All heat transfer, including the envelope heat transfer and internal heat source, was considered as one heat source in each zone. For analysis convenience, we assumed the heat source in the left tunnel as positive, and the heat source of the right tunnel could be either negative or positive such that we could discuss the scenario of two opposing heat sources and the scenario of one heat sink and one heat source. As shown in Fig. 1, there would be two realizations for the building configurations.

2.1 Description of mathematical model

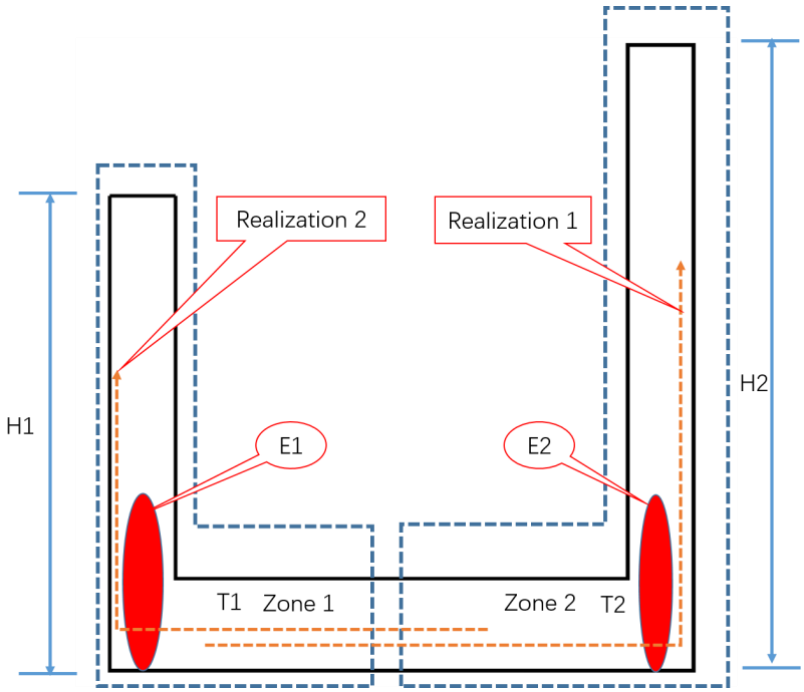

Fig. 1. Schematics of a typical two-zone underground structure.

For realization 1, the conservation of mass is as follows:

$$q_1 = q_2 \tag{2-1}$$

In realization 1, the air flow enters from zone 1 to zone 2. Hence, the thermal pressure in zone 1 will resist the airflow, while the thermal pressure in zone 2 will assist the air flow. Based on the looped method, the sum of the buoyancy pressure balances the flow-element pressure losses [8, 46].The pressure balance equation is as follows:

$$-\frac{T_1-T_a}{T_a}\rho_a g H_1 + \frac{T_2-T_a}{T_a}\rho_a g H_2 = S_1 q_1^2 + S_2 q_2^2 \tag{2-2}$$

The heat gain of the internal thermal mass is equal to the heat released by the heat sources minus the heat loss through airflows. The heat balance equation for zones 1 and 2 can be obtained:

$$M_1 C_p \frac{dT_1}{dt} = -q_1 C_p (T_1 - T_a) + E_1 \tag{2-3}$$

$$M_2 C_p \frac{dT_2}{dt} = -q_2 C_p (T_2 - T_1) + E_2 \tag{2-4}$$

From Eqs. 2-1 and 2-2, we can obtain

$$q_1 = q_2 = \sqrt{\frac{-\frac{T_1-T_a}{T_a}\rho_a g H_1 + \frac{T_2-T_a}{T_a}\rho_a g H_2}{S_1+S_2}} \quad (2\text{-}5)$$

Substituting Eq. 2.5 into Eqs. 2-3 and 2-4 results in the following two-dimensional nonlinear ordinary differential equation system:

$$M_1 C_p \frac{dT_1}{dt} = -\sqrt{\frac{-\frac{T_1-T_a}{T_a}\rho_a g H_1 + \frac{T_2-T_a}{T_a}\rho_a g H_2}{S_1+S_2}}\, C_p(T_1-T_a) + E_1 \quad (2\text{-}6)$$

$$M_2 C_p \frac{dT_2}{dt} = -\sqrt{\frac{-\frac{T_1-T_a}{T_a}\rho_a g H_1 + \frac{T_2-T_a}{T_a}\rho_a g H_2}{S_1+S_2}}\, C_p(T_2-T_1) + E_2 \quad (2\text{-}7)$$

The prerequisite for this equation system is $-\frac{T_1-T_a}{T_a}\rho_a g H_1 + \frac{T_2-T_a}{T_a}\rho_a g H_2 > 0$, which means that the thermal pressure in the right tunnel should be greater than that in the left tunnel.

Similarly, we can obtain the mass balance equation for realization 2:

$$q_1 = q_2 \quad (2\text{-}8)$$

In realization 2, the air flow enters from zone 2 to zone 1. Hence, the thermal pressure in zone 2 will resist the airflow, while the thermal pressure in zone 1 will assist the air flow. We can obtain the pressure balance equation:

$$\frac{T_1-T_a}{T_a}\rho_a g H_1 - \frac{T_2-T_a}{T_a}\rho_a g H_2 = S_1 q_1^2 + S_2 q_2^2 \quad (2\text{-}9)$$

Furthermore, the heat balance equation for realization 2 is as follows:

$$M_1 C_p \frac{dT_1}{dt} = -q_1 C_p(T_1-T_2) + E_1 \quad (2\text{-}10)$$

$$M_2 C_p \frac{dT_2}{dt} = -q_2 C_p(T_2-T_a) + E_2 \quad (2\text{-}11)$$

From Eqs. 2-8 and 2-9, we can obtain

$$q_1 = q_2 = \sqrt{\frac{\frac{T_1-T_a}{T_a}\rho_a g H_1 - \frac{T_2-T_a}{T_a}\rho_a g H_2}{S_1+S_2}} \quad (2\text{-}12)$$

Substituting Eq.2.12 into Eqs. 2-10 and 2-11 results in the following two-dimensional nonlinear ordinary differential equation system:

$$M_1 C_p \frac{dT_1}{dt} = -\sqrt{\frac{\frac{T_1-T_a}{T_a}\rho_a g H_1 - \frac{T_2-T_a}{T_a}\rho_a g H_2}{S_1+S_2}}\, C_p(T_1-T_2) + E_1 \quad (2\text{-}13)$$

$$M_2 C_p \frac{dT_2}{dt} = -\sqrt{\frac{\frac{T_1-T_a}{T_a}\rho_a g H_1 - \frac{T_2-T_a}{T_a}\rho_a g H_2}{S_1+S_2}} C_p (T_2 - T_a) + E_2 \quad (2\text{-}14)$$

The prerequisite for this equation system is $-\frac{T_1-T_a}{T_a}\rho_a g H_1 + \frac{T_2-T_a}{T_a}\rho_a g H_2 < 0$, which means that the thermal pressure in the left tunnel should be greater than that in the right tunnel.

2.2 Stability and existence of the system

Assuming $\kappa = \frac{E_2}{E_1}$, $\Delta T_1 = T_1 - T_a, \Delta T_2 = T_2 - T_a$, $n = \sqrt{\frac{\frac{\rho_a g H_1}{T_a}}{S_1+S_2}}$, $\alpha = H_2/H_1$, $E_1 > 0, C_p = 1, M_1 = M_2 = 1$, the nonlinear ordinary differential equation system can be further simplified.

2.2.1 Stability analysis for scenario 1(κ is fixed, α is control parameter)

2.2.1.1 Stability analysis for $\kappa > 0$

First, we begin from the scenario where two heat sources are positive. For status 1,

$$f_1(\Delta T_1, \Delta T_2) = \frac{d\Delta T_1}{dt} = -n\sqrt{\alpha \Delta T_2 - \Delta T_1}\, \Delta T_1 + E_1 \quad (2\text{-}15)$$

$$f_2(\Delta T_1, \Delta T_2) = \frac{d\Delta T_2}{dt} = -n\sqrt{\alpha \Delta T_2 - \Delta T_1}(\Delta T_2 - \Delta T_1) + E_2 \quad (2\text{-}16)$$

For realization 2, Eqs. 2-13 and 2-14 can be simplified as follows:

$$f_3(\Delta T_1, \Delta T_2) = \frac{d\Delta T_1}{dt} = -n\sqrt{\Delta T_1 - \alpha \Delta T_2}(\Delta T_1 - \Delta T_2) + E_1 \quad (2\text{-}17)$$

$$f_4(\Delta T_1, \Delta T_2) = \frac{d\Delta T_2}{dt} = -n\sqrt{\Delta T_1 - \alpha \Delta T_2}\, \Delta T_2 + E_2 \quad (2\text{-}18)$$

In summary，for the scenario with two positive heat sources ($\kappa > 0$), when $0 < \alpha < \frac{1}{1+\kappa}$, the system has one stable fixed point in realization 2; when $\frac{1}{1+\kappa} < \alpha < \frac{5}{4+5\kappa}$, the system has one unstable fixed point in realization 1 and a stable fixed point in

realization 2; when $\frac{5}{4+5\kappa} < \alpha < \frac{5+4\kappa}{5\kappa}$, the system has two stable fixed points; when $\frac{5+4\kappa}{5\kappa} < \alpha < \frac{1+\kappa}{\kappa}$, the system has one stable fixed point in realization 1 and an unstable fixed point in realization 2; when $\frac{1+\kappa}{\kappa} < \alpha$, the system has one stable fixed point in realization 1 and no solution for realization 2. The detailed derivations are provided in Appendices A1 & A2.

2.2.1.2 Stability analysis for $\kappa < 0$

When one heat source and one heat sink exist ($\kappa < 0$), we still can utilize the characteristic equation to evaluate the stability and existence of the nonlinear differential equation system.

Assuming that no fixed point exists in realization 1, the following expression should be complied:

$$\begin{cases} -1 + \alpha + \alpha\kappa < 0 \\ \kappa < 0 \\ \alpha > 0 \end{cases} \quad (2\text{-}19)$$

Therefore, $\kappa \leq -1 \; and \; \alpha > 0 \; or \; -1 < \kappa < 0 \; and \; 0 < \alpha < \frac{1}{1+\kappa}$.

Assuming that a stable fixed point exists in realization 1, the following expression should be complied:

$$\begin{cases} -1 + \alpha + \alpha\kappa > 0 \\ \kappa < 0 \\ \alpha > 0 \\ -5 + \alpha(4 + 5\kappa) > 0 \end{cases} \quad (2\text{-}20)$$

Therefore, $-\frac{4}{5} < \kappa < 0$ and $\alpha > \frac{5}{4+5\kappa}$.

Assuming that an unstable fixed point exists in realization 1, the following expression should be complied:

$$\begin{cases} -1 + \alpha + \alpha\kappa > 0 \\ \kappa < 0 \\ \alpha > 0 \\ -5 + \alpha(4 + 5\kappa) < 0 \end{cases} \quad (2\text{-}21)$$

Therefore, $-1 < \kappa < -\frac{4}{5}$ and $\alpha > \frac{1}{1+\kappa}$, or $-\frac{4}{5} < \kappa < 0$ and $\frac{1}{1+\kappa} < \alpha < \frac{5}{4+5\kappa}$.

Assuming that no fixed point exists in realization 2, the following expression should be complied:

$$\begin{cases} 1+\kappa-\alpha\kappa<0 \\ \kappa<0 \\ \alpha>0 \end{cases} \quad (2\text{-}22)$$

Therefore, $\kappa<-1$ and $0<\alpha<\frac{1+\kappa}{\kappa}$.

Assuming that a stable fixed point exists in realization 2, the following expression should be complied:

$$\begin{cases} 1+\kappa-\alpha\kappa>0 \\ \kappa<0 \\ 5+(4-5\alpha)\kappa>0 \\ \alpha>0 \end{cases} \quad (2\text{-}23)$$

Therefore, $\kappa\leq-1$ and $\alpha>\frac{1+\kappa}{\kappa}$, or $-1<\kappa<0$ and $\alpha>0$.

Assuming that an unstable fixed point exists in realization 2, the following expression should be complied:

$$\begin{cases} 1+\kappa-\alpha\kappa>0 \\ \kappa<0 \\ 5+(4-5\alpha)\kappa<0 \\ \alpha>0 \end{cases} \quad (2\text{-}24)$$

However, this expression system is not true.

In summary, for the scenario of one heat source and one heat sink ($\kappa<0$), different situations should be considered: $\kappa<-1$, $-1<\kappa<-\frac{4}{5}$, and $-\frac{4}{5}<\kappa<0$. Once the interval of κ is fixed, we can evaluate the stability and existence of the fixed point according to the value of α shown in Table 1.

Table 1

Criterion for scenario 1

κ	α	Existence and stability for realization 1	Existence and stability for realization 2
$(0,+\infty)$	$(0,\frac{1}{1+\kappa})$	No	Stable
	$(\frac{1}{1+\kappa},\frac{5}{4+5\kappa})$	Unstable	Stable

	$(\frac{5}{4+5\kappa}, \frac{5+4\kappa}{5\kappa})$	Stable	Stable
	$(\frac{5+4\kappa}{5\kappa}, \frac{1+\kappa}{\kappa})$	Stable	Unstable
	$(\frac{1+\kappa}{\kappa}, +\infty)$	Stable	No
$(-\frac{4}{5}, 0)$	$(0, \frac{1}{1+\kappa})$	No	Stable
	$(\frac{1}{1+\kappa}, \frac{5}{4+5\kappa})$	Unstable	Stable
	$(\frac{5}{4+5\kappa}, +\infty)$	Stable	Stable
$(-1, -\frac{4}{5})$	$(0, \frac{1}{1+\kappa})$	No	Stable
	$(\frac{1}{1+\kappa}, +\infty)$	Unstable	Stable
$(-\infty, -1)$	$(0, \frac{1+\kappa}{\kappa})$	No	No
	$(\frac{1+\kappa}{\kappa}, +\infty)$	No	Stable

2.2.2 Stability analysis for scenario 2 (α is fixed, κ is control parameter)

In this scenario, the characteristic equation is the same as that of scenario 1.

Assuming no fixed point exists in realization 1, the following expression should be complied:

$$\begin{cases} -1 + \alpha + \alpha\kappa < 0 \\ \alpha > 0 \end{cases} \quad (2\text{-}25)$$

Therefore, $\alpha > 0$ and $\kappa < \frac{1-\alpha}{\alpha}$.

Assuming that a stable fixed point exists in realization 1, the following expression should be complied:

$$\begin{cases} -1 + \alpha + \alpha\kappa > 0 \\ \alpha > 0 \\ -5 + \alpha(4 + 5\kappa) > 0 \end{cases} \quad (2\text{-}26)$$

Therefore, $\alpha > 0$ and $\kappa > \frac{5-4\alpha}{5\alpha}$.

Assuming that an unstable fixed point exists in realization 1, the following expression should be complied:

$$\begin{cases} -1+\alpha+\alpha\kappa>0 \\ \alpha>0 \\ -5+\alpha(4+5\kappa)<0 \end{cases} \quad (2\text{-}27)$$

Therefore, $\alpha>0$ and $\frac{1-\alpha}{\alpha}<\kappa<\frac{5-4\alpha}{5\alpha}$.

Assuming that no fixed point exists in realization 2, the following expression should be complied:

$$\begin{cases} 1+\kappa-\alpha\kappa<0 \\ \alpha>0 \end{cases} \quad (2\text{-}28)$$

Therefore, $0<\alpha<1$ and $\kappa<\frac{1}{-1+\alpha}$, or $\alpha>1$ and $\kappa>\frac{1}{-1+\alpha}$.

Assuming that a stable fixed point exists in realization 2, the following expression should be complied:

$$\begin{cases} 1+\kappa-\alpha\kappa>0 \\ 5+(4-5\alpha)\kappa>0 \\ \alpha>0 \end{cases} \quad (2\text{-}29)$$

Therefore, $0<\alpha\leq\frac{4}{5}\ and\ \kappa>\frac{1}{-1+\alpha}$ or $\frac{4}{5}<\alpha<1\ and\ \frac{1}{-1+\alpha}<\kappa<\frac{5}{-4+5\alpha}$, or $\geq 1\ and\ \kappa<\frac{5}{-4+5\alpha}$.

Assuming that an unstable fixed point exists in realization 2, the following expression should be complied:

$$\begin{cases} 1+\kappa-\alpha\kappa>0 \\ 5+(4-5\alpha)\kappa<0 \\ \alpha>0 \end{cases} \quad (2\text{-}30)$$

Therefore, $\frac{4}{5}<\alpha\leq 1\ and\ \kappa>\frac{5}{-4+5\alpha}$, or $\alpha>1\ and\ \frac{5}{-4+5\alpha}<\kappa<\frac{1}{-1+\alpha}$.

In summary, for scenario 2, different situations should be considered, i.e., $0<\alpha\leq\frac{4}{5}$, $\frac{4}{5}<\alpha<1$, $\alpha=1$, and $\alpha>1$. Once the interval of α is fixed, we can evaluate the stability and existence of the fixed point according to the value of κ shown in Table 2.

Table 2

Criterion for scenario 2

α	κ	Existence and stability	Existence and stability for

		for realization 1	realization 2
$(0,\frac{4}{5})$	$(-\infty,\frac{1}{-1+\alpha})$	No	No
	$(\frac{1}{-1+\alpha},\frac{1-\alpha}{\alpha})$	No	Stable
	$(\frac{1-\alpha}{\alpha},\frac{5-4\alpha}{5\alpha})$	Unstable	Stable
	$(\frac{5-4\alpha}{5\alpha},+\infty)$	Stable	Stable
$(\frac{4}{5},1)$	$(-\infty,\frac{1}{-1+\alpha})$	No	No
	$(\frac{1}{-1+\alpha},\frac{1-\alpha}{\alpha})$	No	Stable
	$(\frac{1-\alpha}{\alpha},\frac{5-4\alpha}{5\alpha})$	Unstable	Stable
	$(\frac{5-4\alpha}{5\alpha},\frac{5}{-4+5\alpha})$	Stable	Stable
	$(\frac{5}{-4+5\alpha},+\infty)$	Stable	Unstable
1	$(-\infty,0)$	No	Stable
	(0,0.2)	Unstable	Stable
	(0.2,5)	Stable	Stable
	$(5,+\infty)$	Stable	Unstable
$(1,+\infty)$	$(-\infty,\frac{1-\alpha}{\alpha})$	No	Stable
	$(\frac{1-\alpha}{\alpha},\frac{5-4\alpha}{5\alpha})$	Unstable	Stable
	$(\frac{5-4\alpha}{5\alpha},\frac{5}{-4+5\alpha})$	Stable	Stable
	$(\frac{5}{-4+5\alpha},\frac{1}{-1+\alpha})$	Stable	Unstable
	$(\frac{1}{-1+\alpha},+\infty)$	Stable	No

2.2.3 Stability analysis for scenario 3 (one heat source at the bottom of the building)

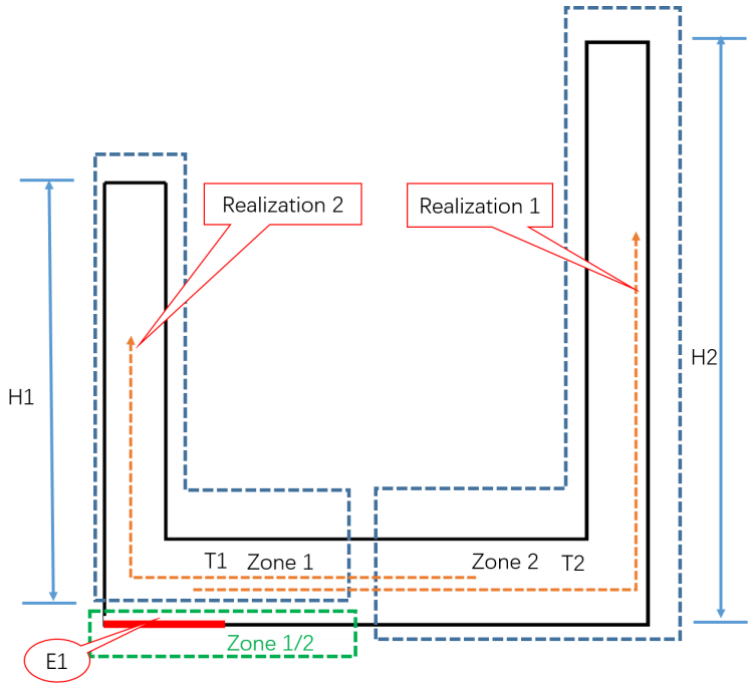

Fig. 2. Schematics of a typical two-zone underground structure with one local heat source.

As illustrated in Fig. 2， for status 1, the heat at the bottom releases to the right tunnel; therefore,

$$f_1(\Delta T_1, \Delta T_2) = \frac{d\Delta T_1}{dt} = -n\sqrt{\alpha\Delta T_2 - \Delta T_1}\,\Delta T_1 \quad (2\text{-}31)$$

$$f_2(\Delta T_1, \Delta T_2) = \frac{d\Delta T_2}{dt} = -n\sqrt{\alpha\Delta T_2 - \Delta T_1}(\Delta T_2 - \Delta T_1) + E_1 \quad (2\text{-}32)$$

For status 2, the heat at the bottom releases to zone 1; therefore,

$$f_3(\Delta T_1, \Delta T_2) = \frac{d\Delta T_1}{dt} = -n\sqrt{\Delta T_1 - \alpha\Delta T_2}(\Delta T_1 - \Delta T_2) + E_1 \quad (2\text{-}33)$$

$$f_4(\Delta T_1, \Delta T_2) = \frac{d\Delta T_2}{dt} = -n\sqrt{\Delta T_1 - \alpha\Delta T_2}\,\Delta T_2 \quad (2\text{-}34)$$

In summary, for the scenario of one heat source at the bottom of the building, because the heat can enter either the left or the right tunnel, two steady states always exist for this scenario. The parameter α will not affect the stability and existence of this building configuration; the detailed derivations are provided in Appendices B1 & B2.

2.3 Model validation

To validate the model, we selected scenario 3 to compare the modeled results with results from a previous study [44] because only this building configuration (one heat source at the bottom with two adiabatic tunnels) has been reported in the literature. The outdoor temperature was 288 K, the air density 1.225 kg/m^3, C_p 1.0 $kJ/(kg \cdot K)$, heat source 1 kW, H_1 5.5 m, H_2 5.5 m, S_{1+2} 37.2933 $kg^{-1} \cdot m^{-1}$, and gravity acceleration g 9.81 m/s^2. The comparison in temperature difference between the proposed model and the validated results from [44] is illustrated in Fig. 3(a); the maximum relative error is 13.2% when the strength of the local heat source is 100 W. The maximum relative error for the flow rate is 15.9%, as indicated in Fig. 3(b), when the strength of the local heat source is 100 W. It is clear that the relative error is small for status 2 compared with status 1. For status 2, the airflow enters from the right stack and is assisted by local buoyancy at the left corner, and displacement ventilation is established. For status 1, the outdoor air enters from the left stack and combats with the local buoyancy at the left corner of the room, and mixed ventilation is established. Hence, the room height should be deducted from the stack height when the buoyancy pressure is calculated in zone 2. After this ratification, the maximum relative error of the flow rate is 12.31%, while the maximum relative error of the temperature difference is 10.39%. In general, the modeled results agree well with the validated results from the previous study.

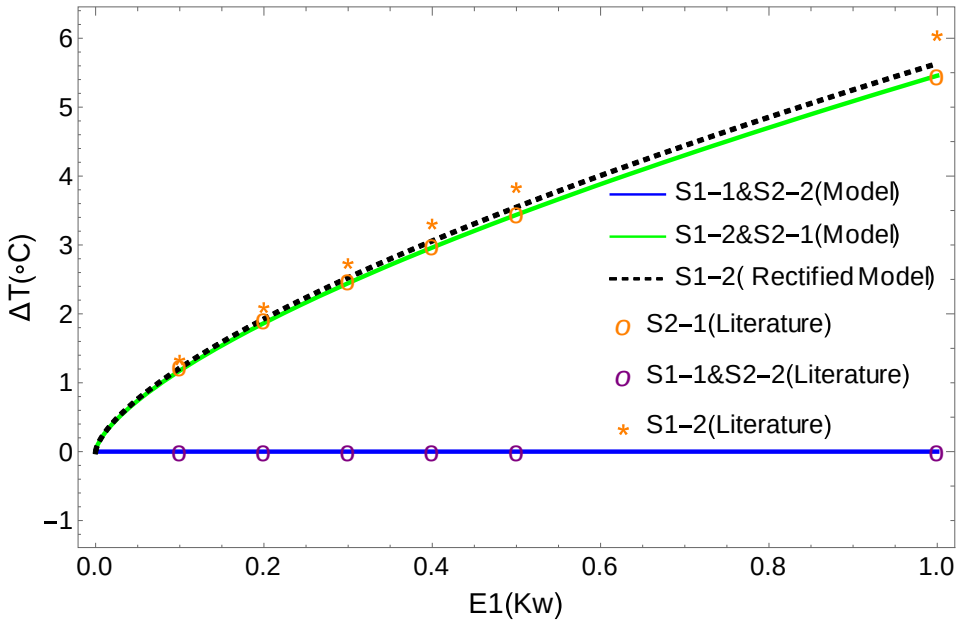

(a)

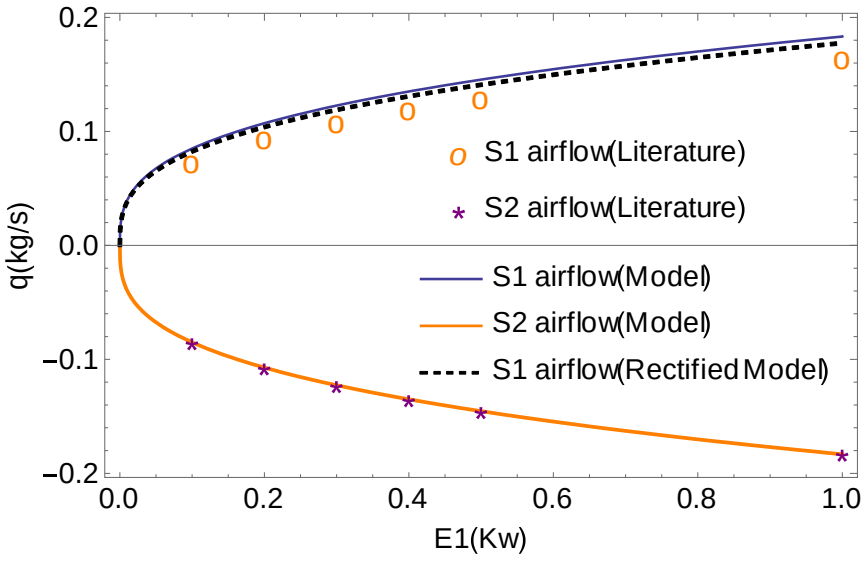

(b)

Fig. 3. Modeled results validation: (a) Temperature comparison between the two-zone model and previous CFD results; (b) Mass flow rates comparison between the two-zone model and previous CFD results. (S1 indicates status1/realization 1, #-(1,2) indicates zone number)

2.4 Graphical representation

To further illustrate the nonlinear dynamical process, we used the fourth-order Runge–Kutta method to numerically solve the differential equation system for different

scenarios. Different initial zone temperatures were used to produce the different trajectories of the system in the phase portrait. We superimposed the vector field and phase portrait together such that the formation of multiple steady states could be observed more straightforwardly. The existence and stability of the nonlinear ordinary equation system can be demonstrated by the phase portrait and vector field. Furthermore, the results agree well with the analysis from the characteristic equation of the differential equation system. We selected some typical cases to demonstrate this dynamical process: Section 2.4.1 describes scenario 1, where the strength of the heat ratio is fixed, and the height ratio is the control parameter; Section 2.4.3 presents scenario 2, where the height ratio is fixed and the heat ratio is the control parameter; Section 2.4.3 investigates scenario 3, where a single heat source exists at the bottom of the building with two adiabatic tunnels.

2.4.1 Same heat source strength, different stack heights (scenario 1)

For scenario 1, we used $\kappa = 1$ as an example to graphically study the effect of control parameter α on the stability of the buoyancy ventilation system. All the building configurations, including the building geometry, boundary conditions, and thermal properties, are the same as those of the validated case except the height ratio and number of heat sources. Subsequently, the bifurcation diagram, vector field, and phase portrait were determined. As shown in Fig. 4.(a), when $0 < \alpha < 1/2$, the ventilation system has only one stable solution for realization 2, in which the flow decreases with the increase in α. When $\frac{1}{2} < \alpha < 5/9$, the system has two solutions; the solution for realization 1 is unstable, and that for realization 2 is stable. The flow rates for realization 1 increases with α, and the flow rates for realization 2 decreases with the increase in α. When $5/9 < \alpha < 9/5$, the system has two stable solutions; within this interval, both equilibrium solutions may occur. Under the same conditions, the system can be transferred from one steady state to another steady state with the

appropriate disturbance. When $\frac{9}{5} < \alpha < 2$, realization 1 remains stable, while realization 2 changes from stable to unstable. With the increase in α, the flow rates for realization 1 increases, while that for realization 2 approaches zero gradually. When $\alpha > 2$, the system has only one stable equilibrium solution for realization 1. Therefore, when α is 1/2, 5/9, 9/5, or 2, bifurcation will occur when the stability and existence of solutions of the underground buoyancy ventilation system change at these points.

Fig. 4(b) shows a bifurcation diagram of the two-zone air temperature as a function of α. When $0 < \alpha < 1/2$, only status 2 has a stable solution, and the fluid flows from zone 2 to zone 1. With the increase in α, the temperatures of both zones increase, which is consistent with the decrease in mass flow rate in Fig. 4(a). Because the mass flow rate decreases and the heat strength of the heat sources remains constant, the indoor temperature will increase such that the heat balance can be satisfied. When $\frac{1}{2} < \alpha < 5/9$, the ventilation system has two solutions, realization 1 is an unstable solution; the temperature difference between the two zones increases with α, and the temperature in each zone decreases continuously. However, the state is not stable, while state 2 remains stable. When $5/9 < \alpha < 9/5$, both realizations are stable. In realization 1, with the increase in α, the temperature difference between the two zones does not change significantly, but the height of tunnel 2 increases. Therefore, the thermal pressure of the system increases, and the mass flow from zone 1 to zone 2 increases continuously, which is consistent with the change trend of the mass flow in Fig. 4(a). In realization 2, with the increase in α, the temperature difference between the two zones does not change significantly, while the indoor air temperature increases. Because the height of tunnel 2 increases while that of tunnel 1 remains constant, the thermal pressure in tunnel 2 increases faster compared with that of tunnel 1. Therefore, the overall thermal pressure in the system decreases, thereby resulting in a decrease in mass flow rate, as shown in Fig. 4(a). When $9/5 < \alpha < 2$, status 1 remains stable, while status 2 changes from stable to unstable. With the increase in α, the temperature in the two zones for realization 1 continues to decrease, while the temperature difference between the two

zones does not change significantly. Therefore, when α increases, the height of tunnel 2 increases and the overall thermal pressure increases, thereby resulting in an increase in the overall mass flow, as illustrated in Fig. 4(a). For realization 2, as the height of tunnel 2 increases, the thermal pressure in tunnel 2 continues to increase, and the direction of thermal pressure in tunnel 2 is opposite to the direction of flow for realization 2. Therefore, the resistance of the thermal pressure ventilation system will continue to increase. The airflow of the system will decrease continuously until α is approximately 2. At this time, the height of the tunnel 2 is twice that of tunnel 1, and the ventilation of the system is approximately zero. At this time, the temperatures of zones 1 and 2 are approximately infinite. It is impossible to achieve a near infinity temperature, which represents an unstable solution. When $\alpha > 2$, no solution exists for realization 2, while realization 1 is stable. For realization 1, the temperature difference between the two zones is not obvious, while the air temperature in both zones decreases. This is due to the increasing height of tunnel 2, which results in the increase in overall thermal pressure in the system. The increase in the overall thermal pressure will increase the overall ventilation, which is consistent with the change trend of airflow in Fig. 4(a).

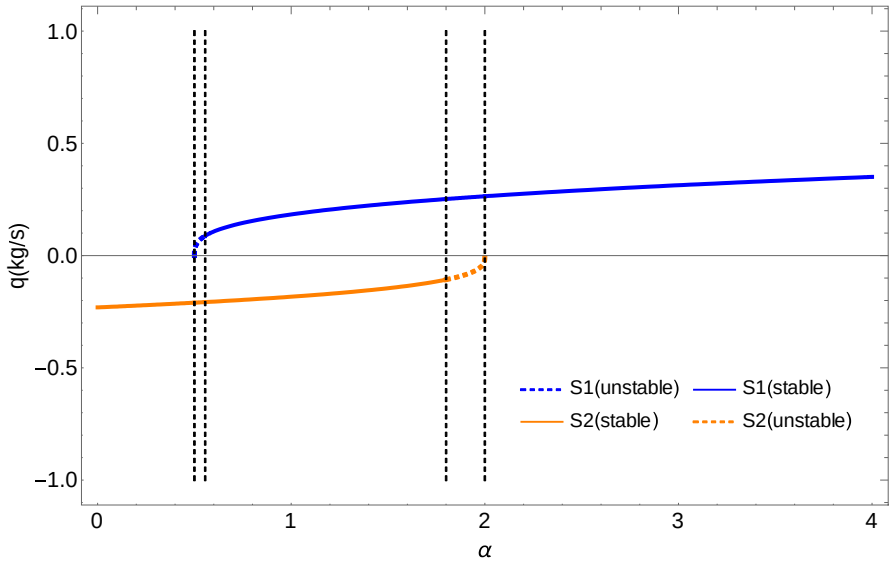

(a)

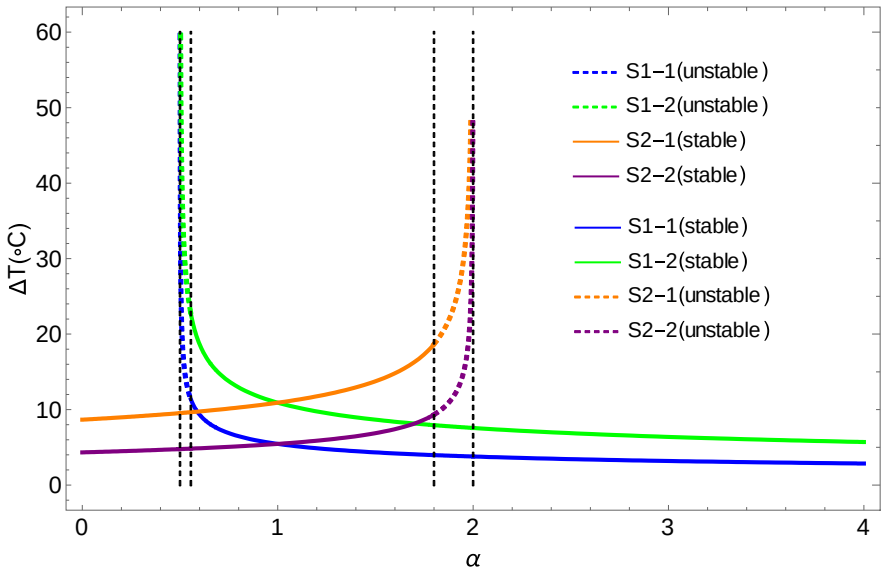

(b)

Fig. 4. Bifurcation diagram for scenario1 ($\kappa = 1$): (a). Bifurcation diagram of mass flow rates; (b). Bifurcation diagram of temperature difference.

The analysis and description process above were used to analyze how α affects the equilibrium results. In the vector field and phase portrait, we compared the formation process of the system from the initial condition to the steady state under different ranges of the control parameter α. Based on the bifurcation diagram, five typical values of α were selected, which were 0.4, 0.54, 1.2, 1.9, and 3. In Fig. 5(a), only a stable fixed point appeared; all different initial conditions converged to the same steady state. As shown in Fig. 5 (b), a straight line $\Delta T_2 = \Delta T_1/\alpha$ appeared, which divided the vector field into two parts. The part above represents realization 1, where the flow enters from the left tunnel and exits from the right tunnel. For the phase plane below the straight line, airflow enters from the right tunnel and exits from the left tunnel, which corresponds to realization 2. Unless the initial condition is exactly equal to the fixed point in realization 1, the trajectories will converge to the stable fixed point in realization 2. This can be realized by solving Eqs.2-15 and 2-16 or Eqs. 2-17 and 2-18 through the fourth-order Runge–Kutta method. For the initial condition above the straight line ($\Delta T_2 = \Delta T_1/\alpha$), the flow direction changes when the trajectories cross the straight line, as indicated in Fig. 5(b). However, for the initial condition below the straight line, the flow will remain in the same direction until it converges to the same

fixed point. As shown in Fig. 5(c), for $\alpha = 1.2$, two stable fixed points appear in the phase plane, where the initial conditions separated by the straight line will converge to the corresponding fixed point. No flow direction changes will occur provided that no large disturbance occurs. As shown in Fig. 5(d), two fixed points exist in the phase plane. However, the fixed point in realization 2 is not stable. All the initial conditions except the exact fixed point will follow the trajectories and converge to the fixed point in realization 1. In fact, even though a fixed point exists in realization 2, the state cannot exist in the real world because the initial condition cannot exactly the same as the fixed point. Similar to that shown in Fig. 5(b), the initial conditions below the straight line ($\Delta T_2 = \Delta T_1/\alpha$) will experience a direction change when the trajectories cross the straight line, as illustrated in Fig. 5(d). The phase portrait indicated in Fig. 5(e) shows that only a stable fixed point exists for the entire phase plane when $\alpha = 3$. All initial conditions will eventually converge to the fixed point.

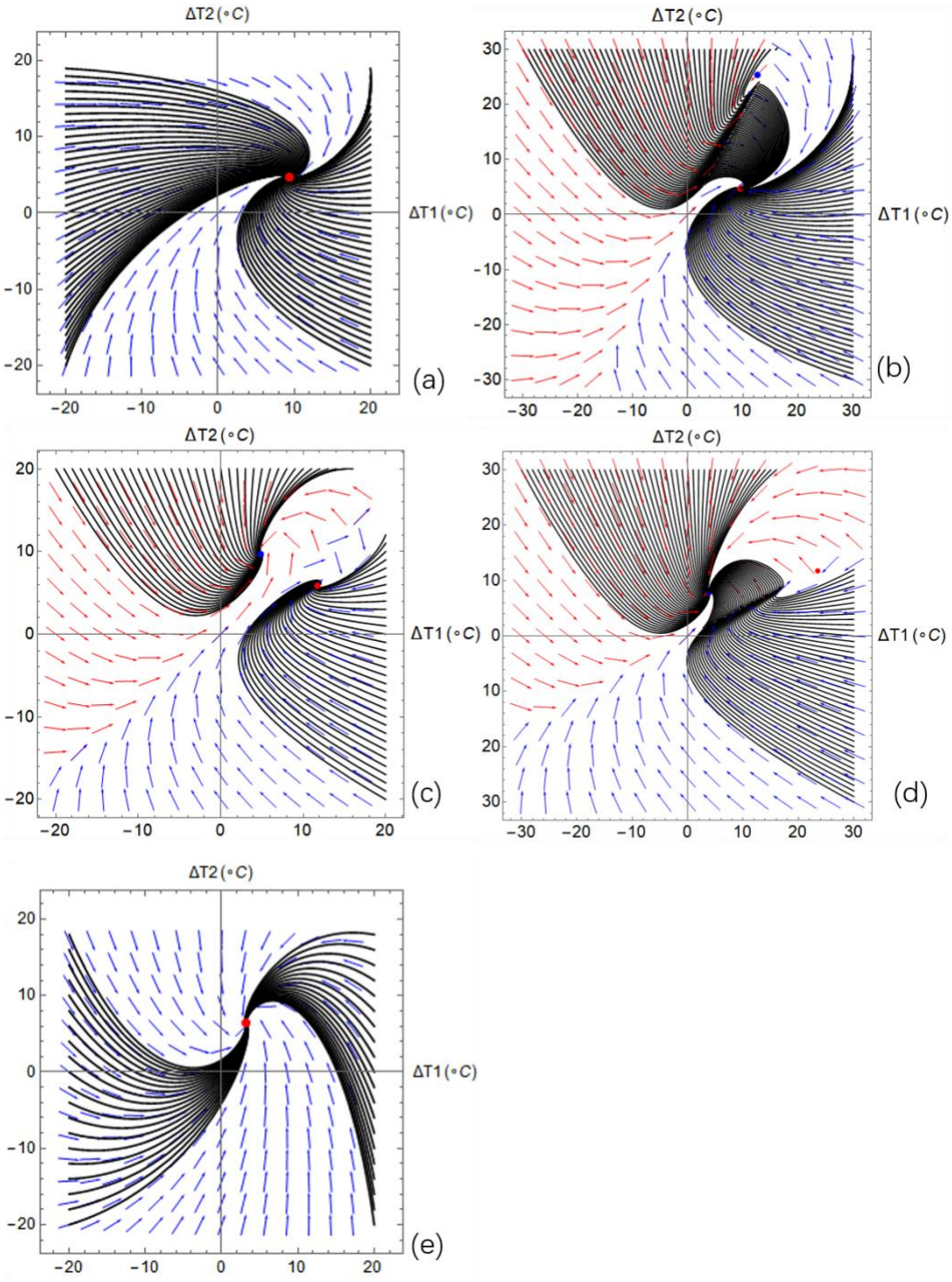

Fig. 5. Phase portrait and vector field for scenario 1: (a). Phase portrait and vector field for $\kappa = 1, \alpha = 0.4$; (b). Phase portrait and vector field for $\kappa = 1, \alpha = 0.54$;(c). Phase portrait and vector field for $\kappa = 1, \alpha = 1.2$;(d).Phase portrait and vector field for $\kappa = 1, \alpha = 1.9$; (e). Phase portrait and vector field for $\kappa = 1, \alpha = 3$

2.4.2 Same stack height (Scenario 2)

For scenario 2, we used $\alpha = 1$ as an example to graphically study the effect of control parameter κ on the stability of the buoyancy ventilation system. As shown in Fig. 6(a), when$\kappa < 0$, only one stable solution exists for realization 2. When $0 < \kappa < 0.2$, the ventilation system has a stable solution for realization 2 and an unstable solution for realization 1. The flow rate for realization 2 is a fixed value, while that for realization 1 increases with κ. When $0.2 < \kappa < 5$, the system has two stable solutions; both equilibrium solutions may appear depending on the initial conditions. Under the same conditions, the system can be transferred from one stable solution to another with the appropriate disturbance. When $5 < \kappa$, state 1 remains stable, while state 2 changes from stable to unstable. With the increase in κ, the flow rate for realization 1 increases. Therefore, the flow bifurcation will occur when κ is 0, 0.2, or 5. The stability of the solution changes at the corresponding points.

Fig. 6(b) shows a bifurcation diagram of the two-zone air temperature as a function of κ. When $\kappa < 0$, only realization 2 has a stable solution, where zone 2 contains a heat sink and zone 1 acts as a heat source. Fluid flows from zone 2 to zone 1. With the increase in the heat ratio, the air temperatures in both zones increase continuously, but the temperature difference between the two zones remains constant, which is consistent with the airflow results in Fig 6(a). When the temperature difference is constant, because the height of the shaft does not change, the thermal pressure of the system remains unchanged. Therefore, the mass flow rate remains unchanged. When $0 < \kappa < 0.2$, an unstable solution exists for realization 1, while a stable solution for realization 2. For realization 1, the temperature difference between the two zones increases with the increase in heat ratio. When $0.2 < \kappa < 5$, two stable solutions exist. For realization 1, the temperature difference between the two zones continues increasing. However, the air temperature of zone 1 decreases, while the temperature of zone 2 increases. The heat released to zone 1 does not change with the increase in outdoor air flow rate;

therefore, the temperature decreases. For zone 2, although the mass flow rate increases, the heat released to zone 2 increases with κ. Therefore, the temperature of zone 2 increases. When $5 < \kappa$, realization 1 remains stable, while realization 2 changes from stable to unstable. For realization 1, the temperature difference between the two zones continues to increase, which is due to the increase in mass flow rate in the interval of $0.2 < \kappa < 5$. For realization 2, because the temperatures of both zones will increase to infinite, which is not achievable, the equilibrium solution can be obtained.

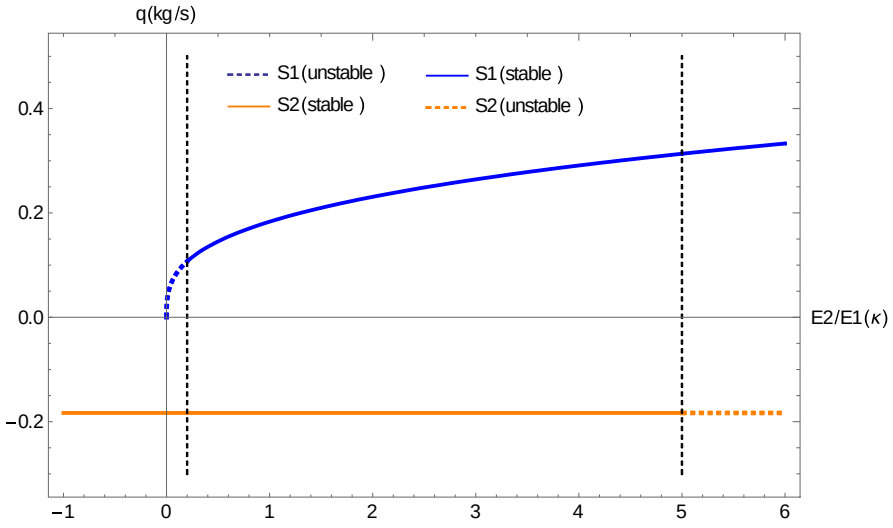

(a)

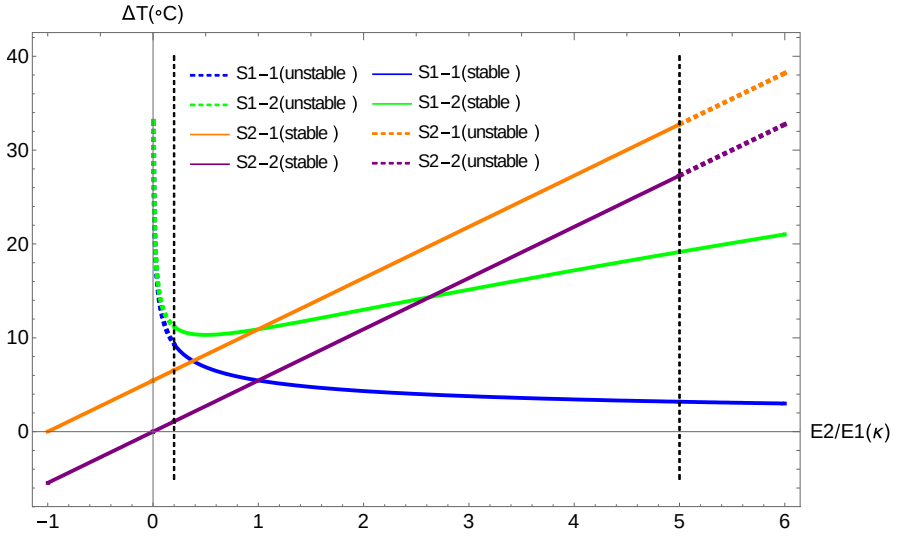

(b)

Fig. 6. Bifurcation diagram for scenario 2($\alpha = 1$): (a). Bifurcation diagram of mass flow rates; (b). Bifurcation diagram of temperature difference.

The analysis and description process above were used to study the effect of κ on the equilibrium results. In the vector field and phase portrait, the typical value of κ

was selected based on the bifurcation diagram to compare the dynamical process of the system from the initial condition to the steady state. Fig. 7(a) describes that all the initial values will follow the corresponding trajectory and converge to the same stable fixed point when $\kappa = -1$. Fig. 7(b) reveals that two fixed points exist in the phase plane when $\kappa = 0.1$. The fixed point in realization 1 is unstable, while all the initial conditions, except the fixed point for realization 1, will converge to the stable fixed point in realization 2. For the initial value above the straight line ($\Delta T_2 = \Delta T_1/\alpha$), they have to cross the straight line where the flow direction is changed. Fig.7(c) shows that two stable fixed points exist at both sides of the straight line ($\Delta T_2 = \Delta T_1/\alpha$). All the initial values will follow their trajectories and converge to the respective fixed points unless the disturbances are imposed. Fig. 7(d) shows that two fixed points exist when $\kappa = 6$. The fixed point in realization 2 is unstable, while the fixed point in realization 1 is stable. Furthermore, the initial value below the straight line ($\Delta T_2 = \Delta T_1/\alpha$) must experience a change in flow direction before it reaches the stable fixed point in realization 1.

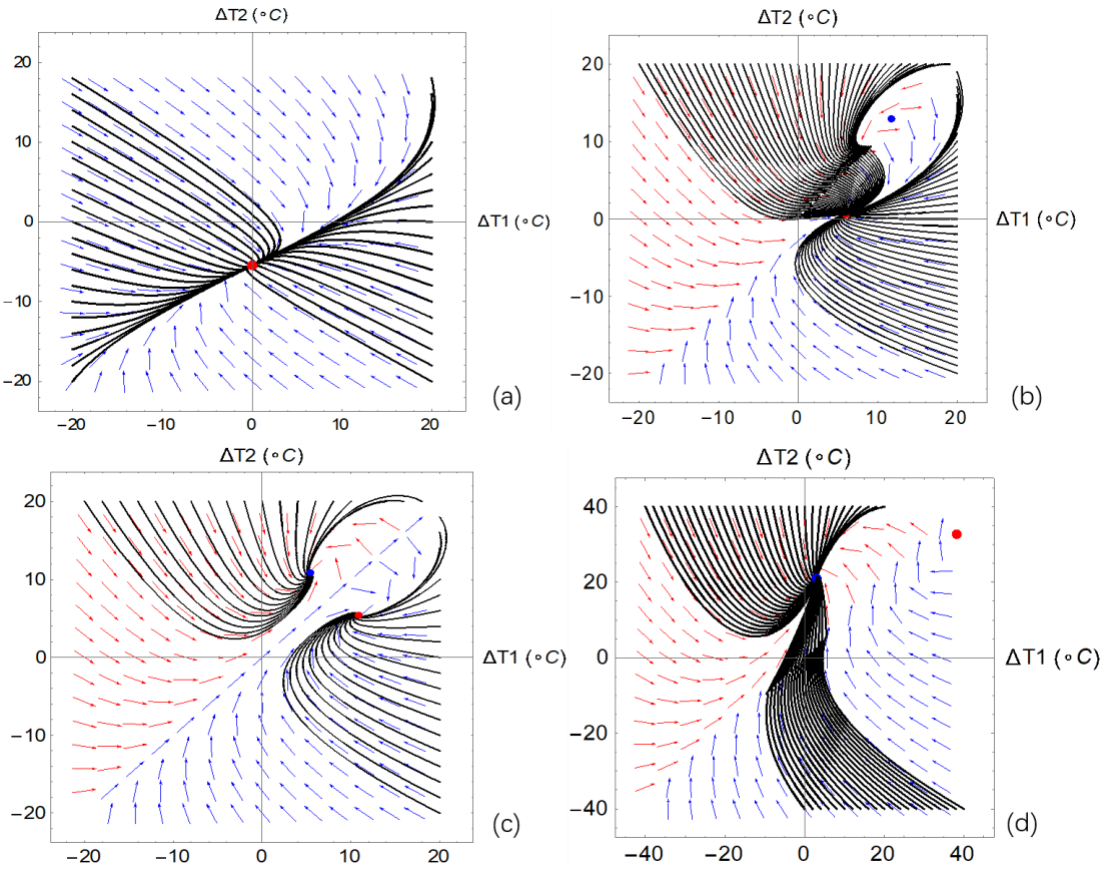

Fig. 7. Phase portrait for scenario 2: (a). Phase portrait and vector field for $\kappa = -1, \alpha = 1$; (b). Phase portrait and vector field for $\kappa = 0.1, \alpha = 1$;(c). Phase portrait and vector field for $\kappa = 1, \alpha = 1$;(d). Phase portrait and vector field for $\kappa = 6, \alpha = 1$.

2.4.3 Single heat source at the bottom of the building (scenario 3)

For scenario 3, all of the parameters are the same as those of the validated case. As proven in Section 2.2.3, no bifurcation exists in this building configuration. Hence, no bifurcation diagram is available in this scenario. However, Fig. 3 shows the changes in airflow rate and air temperature with the change in the strength of the local heat source. Furthermore, the phase portrait and vector field were determined according to the fourth Runge–Kutta method. As illustrated in Fig. 8, two stable fixed points exist in the phase plane. The vector field is divided by the straight line ($\Delta T_2 = \Delta T_1/\alpha$), which represents the balance in thermal pressure between zones 1 and 2.Above the straight line, all the flow will reach the fixed point in realization 1, while the initial value below the straight line will converge to the fixed point in realization 2. If the initial value is below the

straight line, but the fixed point in realization 1 is to be reached, then disturbance has to be imposed such that the phase portrait can be changed for a period of time. When the disturbance disappeared, if the air temperature is located at the top of the straight line, then it can reach the fixed point in realization 1. The disturbance can be the wind effect or mechanical fan power. In other words, this phase portrait is drafted according to the fixed building configurations, which include the building geometry, boundary conditions, and all physical properties. The patterns of the phase portrait and vector field will change according to the building configuration. However, if the derived criterion based on the heat ratios and height ratios is adhered, the general trend will follow that of the criterion, e.g., the number of fixed points and their stability.

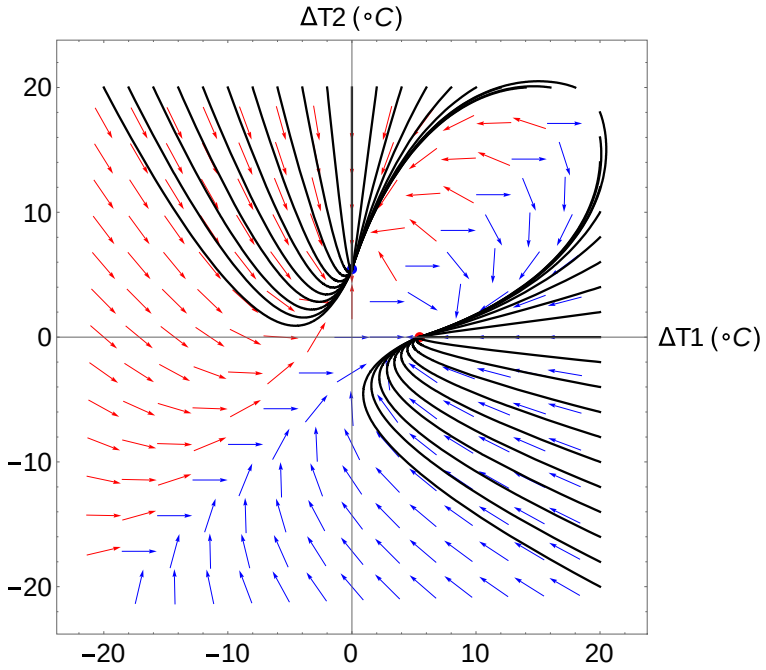

Fig. 8. Phase portrait and vector field for scenario 3 (one local heat source at the bottom).

3. Case study

In this section, the natural ventilation of a hydropower station in Xinjiang is used as an example to analyze the polymorphism of buoyancy ventilation. As shown in Figs. 9 (a) and 9 (b), four generators were used in the hydropower station. The main heating equipment in the plant includes generators, busbar cables, main transformers, lightings,

and control cabinets. As shown in Fig. 9(b), the transportation tunnel is on the left. Generators and other main equipment are in the main workshop. The outlet tunnel of a busbar cable and exhaust shaft is shared. The generator measures 3.6 m in diameter and 1.2 m in height; the main factory measures 36 m (L) × 9 m (W) × 8 m (H); the transportation tunnel measures 3.1 m (L) × 4.5 m (W) in cross section, 170 m in length, and 86 m in height; the exhaust tunnel measures 140 m in height, and the diameter of the exhaust shaft is approximately 6 m.

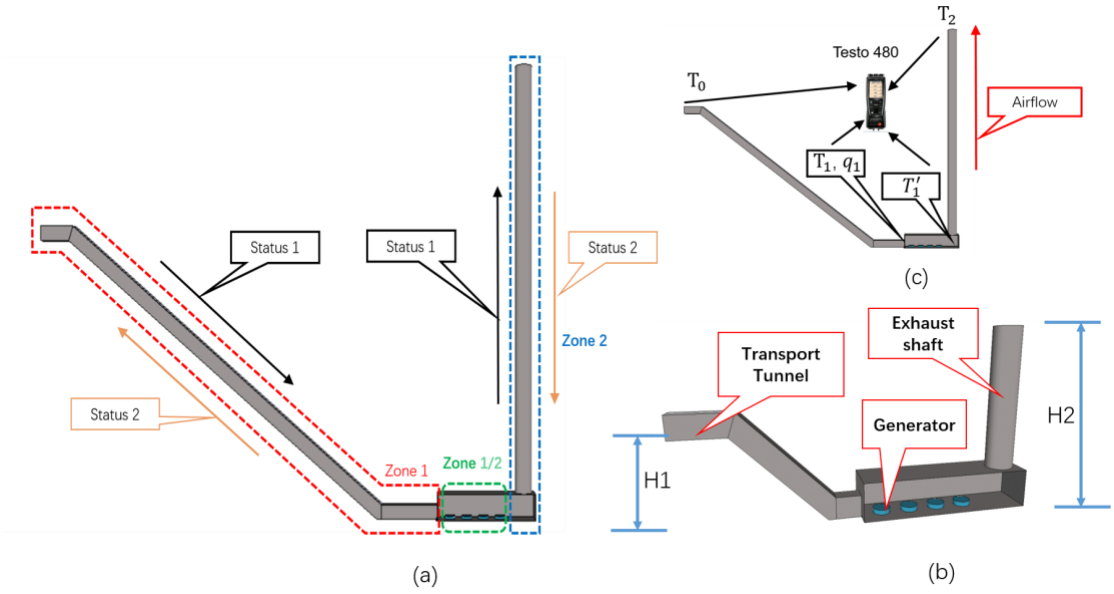

Fig. 9. Basic information of the hydropower station.

Field measurements were conducted in the summer, and the censoring points and setups are shown in Fig. 9(c). Testo 480 was used to capture the air temperature and air velocity. The airflow rate was measured at the junction between the transportation tunnel and the main factory. The mean mass flow rate is 3.22 m^3/s; the outdoor temperature T_0 is 23.2 °C; the temperature at the entrance of the factory T_1 is 14.4 °C; T_1' *and* T_2 are 25.6 °C and 22.1 °C, respectively. The temperature changed significantly in both the transportation tunnel and the exhaust tunnel. However, for the nonlinear dynamical analysis, we still used the well-mixed assumption, because this assumption will not significantly affect the solution multiplicity analysis. Based on simple calculations, the heat loss through the transportation tunnel is 34.9 kW, the

overall heat gain from the factory is 44.4 kW, and the overall heat loss through the exhaust tunnel is 13.9 kW; $H_1$is 86 m and H_2 is 140 m; hence, α is 1.628, and S is 1.55 $kg^{-1} \cdot m^{-1}$. The outdoor temperature is 23.2 °C, air density 1.22 kg $\cdot m^{-3}$, and C_p 1.01 kJ/$(kg \cdot K)$. The thermal mass of the air inside the tunnel was considered without considering other building elements. The thermal masses in the transportation tunnel, factory, and exhaust tunnel are 2372, 2592, and 3956 kg, respectively.

For realization 1, the airflow entered from the transportation tunnel, and the thermal mass and overall heat gain from the factory were transferred to zone 2; therefore, M_1 is 2372 kg, M_2 is 6548 kg, E_1 is -34.9 kW, and E_2 is 30.1 kW. Therefore, we have

$$M_1 C_p \frac{d\Delta T_1}{dt} = -\sqrt{\frac{\rho_a g H_1}{T_a(S_1+S_2)}}\sqrt{-\Delta T_1 + \Delta T_2 \alpha}\, C_p \Delta T_1 + E_1 \quad (3\text{-}1)$$

$$M_2 C_p \frac{dT_2}{dt} = -\sqrt{\frac{\rho_a g H_1}{T_a(S_1+S_2)}}\sqrt{-\Delta T_1 + \Delta T_2 \alpha}\, C_p (\Delta T_2 - \Delta T_1) + E_2 \quad (3\text{-}2)$$

The root of the characteristic equation of the differential equation is $\lambda_1 = -0.0034$, $\lambda_2 = -0.0004321$. Both roots are real distinct negative value; hence, a stable fixed point exists for realization 1.

For realization 2, the airflow entered from the exhaust tunnel, and the thermal mass and overall heat gain from the factory were transferred to zone 1; therefore, M_3 is 4964 kg, M_4 is 3956 kg, E_3 is 9.5 kW, and E_3 is -13.9 kW. We have

$$M_3 C_p \frac{d\Delta T_1}{dt} = -\sqrt{\frac{\rho_a g H_1}{T_a(S_1+S_2)}}\sqrt{\Delta T_1 - \alpha \Delta T_2}(\Delta T_1 - \Delta T_2) + E_3 \quad (3\text{-}3)$$

$$M_4 C_p \frac{d\Delta T_2}{dt} = -\sqrt{\frac{\rho_a g H_1}{T_a(S_1+S_2)}}\sqrt{\Delta T_1 - \alpha \Delta T_2}\, \Delta T_2 + E_4 \quad (3\text{-}4)$$

The root of the characteristic equation of the differential equation is $\lambda_1 = -0.001765$, $\lambda_2 = -0.0005075$. Both roots are real distinct negative values; hence, a stable fixed point exists for realization 2 as well.

Based on Eqs. 3-1, 3-2, 3-3, and 3-2, we numerically solved these differential equation systems. The vector field and phase portrait are shown in Fig.10. The stability and existence of the system obtained from the numerical computation is the same as those from the nonlinear dynamical analysis. Two stable fixed points exist, and the

vector field is divided by the straight line ($\Delta T_2 = \Delta T_1/\alpha$).

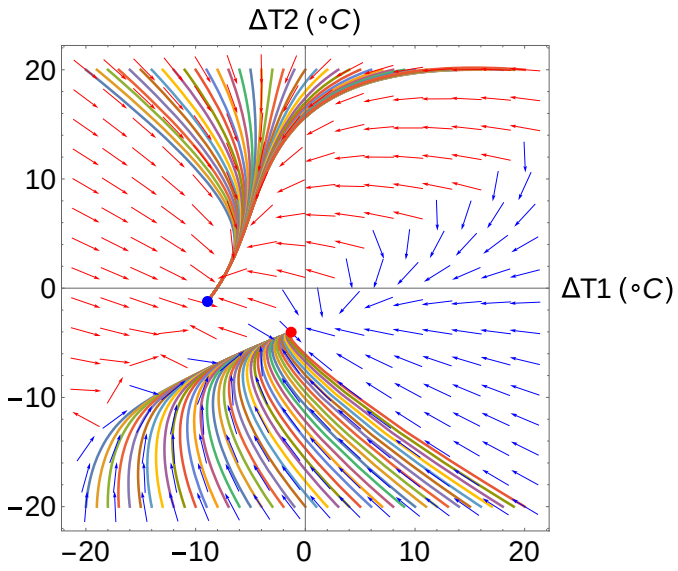

Fig. 10. Phase portrait and vector field for the dynamic system of buoyancy ventilation in the hydropower station

In fact, we can use the derived criterion in scenario 1 to evaluate the stability and existence of fixed points:

When $\kappa < -1$: if $0 < \alpha < \frac{1+\kappa}{\kappa}$, no fixed point exists for realizations 1 and 2; if $\alpha > \frac{1+\kappa}{\kappa}$, no fixed point exists for realization 1but a stable fixed point exists for realization 2.

In scenario 1, we assume that E_1 is constantly positive, while in this case study, we have a negative value for E_1. Hence, both realizations 1 and 2 in the case study corresponds to realization 2 in the criterion.

For realization 1 in the case study, $E_1$is negative, $\kappa = \frac{E_1}{E_2} = -1.159468$, and $\alpha = \frac{H_1}{H_2} = 0.614286$; $\frac{1+\kappa}{\kappa} = 0.1375358$, that is $\alpha > \frac{1+\kappa}{\kappa}$. Therefore, a stable fixed point exists according to the criterion. At the same time, when H_2 remains unchanged, if the height of the left traffic tunnel H_1 is lower than 19.26 m ($\alpha < \frac{1+\kappa}{\kappa}$), this fixed point will not exist.

For realization 2 in the case study, E_4 is negative, $\kappa = \frac{E_4}{E_3} = -1.46316$, and $\alpha = \frac{H_2}{H_1} = 1.627907$; $\frac{1+\kappa}{\kappa} = 0.3165468$, that is $\alpha > \frac{1+\kappa}{\kappa}$. Therefore, a stable fixed point exists according to the criterion. At the same time, when H_1 remains unchanged, if the height of the left traffic tunnel H_2 is lower than 27.2 m ($\alpha < \frac{1+\kappa}{\kappa}$), this fixed point will not exist.

From the analysis and verification above, it can be concluded that the criterion is applicable to the evaluation of buoyancy ventilation polymorphism of two-zone underground buildings. If the specific heat source ratio, height ratio, and flow direction are known, then the existence and stability of the solution can be evaluated according to the criterion. In the design stage, according to the criterion, the natural ventilation of buildings can be optimized by selecting the appropriate height ratio of the shaft and the distribution of heat sources to avoid unfavorable solutions and induce favorable solutions.

4. Conclusions

In summary, nonlinear dynamical analysis was performed to study the buoyancy ventilation of a typical two-zone underground building with different building configurations. One dimensional model that described the buoyancy ventilation of the two-zone underground buildings was proposed and validated by results from previous studies. The model comprised two groups of mathematical nonlinear ordinary differential equation systems. Three different scenarios were studied based on the differential equation systems, and the corresponding criterion for the stability and existence of fixed points for the underground buoyancy ventilation was derived mathematically. The criterion was based on the heat ratio (κ) and height ratio (α). For scenario 1 (κ was fixed, control α) and scenario 2 (α was fixed, control κ), the criterion is summarized in Tables 1 and 2. For scenario 3 (one heat source at the bottom

of the building, control α), two stable fixed points appeared.

Subsequently, the bifurcation diagram, phase portrait, and vector field for the three scenarios were produced based on numerical computation by applying the fourth Runge–Kutta method, which produced the similar result as the characteristic equations.

Finally, a case study was conducted based on a real project with field measurements, which demonstrated the use of the nonlinear dynamical analysis method to evaluate the stability and existence of fixed points for the buoyancy ventilation in a hydropower station. This case study served as a validation case for the derived criterion, which demonstrated its capability in predicting the existence and stability of fixed points in the buoyancy ventilation of underground buildings.

Acknowledgement

The authors acknowledge the support from National Natural Science Foundation of China (NSFC) (51678088, 51178482, 51578087)and National Key R&D Program of China（2017YFB0903700）. Yanan Liu also especially thanks for the scholarship provided by China Scholarship Council (CSC student ID: 201706050003).

Appendix A1 Dynamical analysis of Eqs.2-15 and 2-16

Denote the steady state solution(fixed point) of realization 1(Eqs.2-15 and 2-16) is $\left(\overline{\Delta T_1},\ \overline{\Delta T_2}\right)$, we can obtain：

$$E_1 = n\sqrt{\alpha\overline{\Delta T_2} - \overline{\Delta T_1}}\,\overline{\Delta T_1}, \quad \text{（A1）}$$

$$E_2 = -n\sqrt{\alpha\overline{\Delta T_2} - \overline{\Delta T_1}}\,(\overline{\Delta T_1} - \overline{\Delta T_2}) \quad \text{（A2）}$$

Eq.(A1)divided by Eq.(A2)：

$$\frac{E_1}{E_2} = \frac{\overline{\Delta T_1}}{\overline{\Delta T_2} - \overline{\Delta T_1}} \quad \text{（A3）}$$

Substituting $\frac{E_2}{E1} = \kappa$ into Eq.(A3) and simplifying the equation, we obtain:

$$\overline{\Delta T_2} = \left(1 + \frac{E_2}{E_1}\right)\overline{\Delta T_1} = (1+\kappa)\,\overline{\Delta T_1} \quad \text{（A4）}$$

Substituting Eq.(A4) into Eqs.2-15 and 2-16，Let$\frac{d\Delta T_1}{dt}$ and $\frac{d\Delta T_2}{dt}$ be zero，fixed point can be obtained：

$$\overline{\Delta T_1} = \frac{E_1}{n^{2/3}(-E_1+E_1\alpha+E_2\alpha)^{1/3}} = \frac{E_1}{n^{2/3}(-E_1+E_1\alpha+E_1\alpha\kappa)^{1/3}} \quad \text{（A5）}$$

$$\overline{\Delta T_2} = \frac{(E_1+E_2)}{E_1}\left(\frac{E_1}{n^{2/3}(-E_1+E_1\alpha+E_2\alpha)^{1/3}}\right) = \frac{E_1+E_1\kappa}{n^{2/3}(-E_1+E_1\alpha+E_1\alpha\kappa)^{1/3}} \quad \text{（A6）}$$

To analyze the stability of the nonlinear ordinary differential equations above, we need to linearize the equations at the fixed point, and analyze their existence and stability according to the characteristic equation. Eqs.2-15 and 2-16 can be written as Taylor expansions form at the fixed point $(\overline{\Delta T_1}, \overline{\Delta T_2})$：

$$f_1(\Delta T_1, \Delta T_2) = f_1(\overline{\Delta T_1}, \overline{\Delta T_2}) + \frac{\partial f_1}{\partial \Delta T_1}|_{\substack{\Delta T_1=\overline{\Delta T_1}\\ \Delta T_2=\overline{\Delta T_2}}}(\Delta T_1 - \overline{T_1}) + \frac{\partial f_1}{\partial \Delta T_2}|_{\substack{\Delta T_1=\overline{\Delta T_1}\\ \Delta T_2=\overline{\Delta T_2}}}(\Delta T_2 - \overline{\Delta T_2})$$

（A7）

$$f_2(\Delta T_1, \Delta T_2) = f_2(\overline{\Delta T_1}, \overline{\Delta T_2}) + \frac{\partial f_2}{\partial \Delta T_1}|_{\substack{\Delta T_1=\overline{\Delta T_1}\\ \Delta T_2=\overline{\Delta T_2}}}(\Delta T_1 - \overline{T_1}) + \frac{\partial f_2}{\partial \Delta T_2}|_{\substack{\Delta T_1=\overline{\Delta T_1}\\ \Delta T_2=\overline{\Delta T_2}}}(\Delta T_2 - \overline{\Delta T_2})$$

（A8）

For the steady state，$\frac{d\Delta T_1}{dt}$ and $\frac{d\Delta T_2}{dt}$ is equal to zero. Thus $f_1\left(\overline{\Delta T_1},\ \overline{\Delta T_2}\right) = 0$，and $f_2\left(\overline{\Delta T_1},\ \overline{\Delta T_2}\right) = 0$.

Assuming$\alpha_{11} = \frac{\partial f_1}{\partial \Delta T_1}|_{\substack{\Delta T_1=\overline{\Delta T_1}\\ \Delta T_2=\overline{\Delta T_2}}}$，$\alpha_{12} = \frac{\partial f_1}{\partial \Delta T_2}|_{\substack{\Delta T_1=\overline{\Delta T_1}\\ \Delta T_2=\overline{\Delta T_2}}}$，$\alpha_{21} = \frac{\partial f_2}{\partial \Delta T_1}|_{\substack{\Delta T_1=\overline{\Delta T_1}\\ \Delta T_2=\overline{\Delta T_2}}}$，and $\alpha_{22} = \frac{\partial f_2}{\partial \Delta T_2}|_{\substack{\Delta T_1=\overline{\Delta T_1}\\ \Delta T_2=\overline{\Delta T_2}}}$, Eqs. (A7) and (A8) can be written as follows:

$$f_1(T_1, T_2) = \alpha_{11}(T_1 - \overline{T_1}) + \alpha_{12}(T_2 - \overline{T_2}) \quad \text{（A9）}$$

$$f_2(T_1, T_2) = \alpha_{21}(T_1 - \overline{T_1}) + \alpha_{22}(T_2 - \overline{T_2}) \quad \text{（A10）}$$

Written as matrix form：

$$\begin{bmatrix} \frac{dT_1}{dt} \\ \frac{dT_2}{dt} \end{bmatrix} = A_1 \begin{bmatrix} T_1 \\ T_2 \end{bmatrix} + B \quad \text{(A11)}$$

Where $A_1 = \begin{bmatrix} \alpha_{11} & \alpha_{12} \\ \alpha_{21} & \alpha_{22} \end{bmatrix}$, and $B = \begin{bmatrix} -\alpha_{11}\overline{T_1} - \alpha_{12}\overline{T_2} \\ -\alpha_{21}\overline{T_1} - \alpha_{22}\overline{T_2} \end{bmatrix}$. To evaluate the existence and stability of the solution, we have to obtain the eigenvalue of matrix A_1.

The characteristic equation of realization 1 can be easily obtained as follows:

$$\lambda^2 + \frac{n\sqrt{\frac{(E_1(-1+\alpha+\alpha\kappa))^{2/3}}{n^{2/3}}(-5+\alpha(4+5\kappa))\lambda}}{2(-1+\alpha+\alpha\kappa)} + \frac{3}{2}n^{4/3}(E_1(-1+\alpha+\alpha\kappa))^{2/3} = 0 \qquad \text{(A12)}$$

Assuming $\kappa = \frac{E_2}{E_1} > 0$, to ensure that a real solution exists for Eqs. (A5) and (A6), we have $-E_1 + E_1\alpha + E_1\alpha\kappa > 0$. Because the heat source in zone 2 is positive as well, we have $\kappa > 0$. Therefore, $\alpha > \frac{1}{1+\kappa}$.

Assuming $\beta = \frac{n\sqrt{\frac{(E_1(-1+\alpha+\alpha\kappa))^{2/3}}{n^{2/3}}(-5+\alpha(4+5\kappa))}}{2(-1+\alpha+\alpha\kappa)}$, $\gamma = \frac{3}{2}n^{4/3}(E_1(-1+\alpha+\alpha\kappa))^{2/3}$.The root of the characteristic equation (Eq.A12) is the eigenvalue of matrix A_1. The eigenvalue is given as $\lambda_{1,2} = -\beta \pm \sqrt{\beta^2 - 4\gamma}$. Since$E_1(-1+\alpha+\alpha\kappa) > 0$, and $n > 0$, thus $\gamma = \frac{3}{2}n^{4/3}(E_1(-1+\alpha+\alpha\kappa))^{2/3} > 0$. Therefore, $\lambda_{1,2}$ are determined by the real part of β. When $\beta > 0$，the real part of the eigenvalue is negative; otherwise，the real part of the eigenvalue is positive. To ensure the solution of this differential equation is stable, the root of the characteristic equation should be less than zero. That is $-\beta = -\frac{n\sqrt{\frac{(E_1(-1+\alpha+\alpha\kappa))^{2/3}}{n^{2/3}}(-5+\alpha(4+5\kappa))}}{2(-1+\alpha+\alpha\kappa)} < 0$. Therefore, $-5+\alpha(4+5\kappa) > 0$，that is $\alpha > \frac{5}{4+5\kappa}$.

In summary，when $\frac{1}{1+\kappa} < \alpha < \frac{5}{4+5\kappa}$, the real parts of two eigenvalues are positive，the fixed point is unstable；when $\alpha > \frac{5}{4+5\kappa}$，the real parts of two eigenvalues are negative，the fixed point is stable；when $\alpha < \frac{1}{1+\kappa}$，no fixed point exists.

Appendix A2 Dynamical analysis of Eqs.2-17 and 2-18

Denote the steady state solution(fixed point) of realization 2(Eqs.2-17 and 2-18) is

$\left(\overline{\Delta T_1},\ \overline{\Delta T_2}\right)$, we can obtain:

$$E_1 = n\sqrt{\overline{\Delta T_1} - \overline{\alpha \Delta T_2}}\,(\overline{\Delta T_1} - \overline{\Delta T_2}), \quad \text{(A13)}$$

$$E_2 = n\sqrt{\overline{\Delta T_1} - \overline{\alpha \Delta T_2}}\,\overline{\Delta T_2} \quad \text{(A14)}$$

Eq.(A13) divided by Eq.(A14):

$$\frac{E_1}{E_2} = \frac{\overline{\Delta T_1} - \overline{\Delta T_2}}{\overline{\Delta T_2}} \quad \text{(A15)}$$

Substituting $\frac{E_1}{E2} = \frac{1}{\kappa}$ into Eq.(A15), we can obtain:

$$\overline{\Delta T_1} = \left(1 + \frac{E_1}{E_2}\right)\overline{\Delta T_2} = \left(1 + \frac{1}{\kappa}\right)\overline{\Delta T_2} \quad \text{(A16)}$$

Substituting Eq.(A16) into Eqs.2-17 and 2-18, Let $\frac{d\Delta T_1}{dt}$ and $\frac{d\Delta T_2}{dt}$ be zero, fixed point can be obtained:

$$\overline{\Delta T_1} = (1 + E_1/E_2)\frac{E_2}{n^{2/3}(E_1 + E_2 - E_2\alpha)^{1/3}} = \frac{E_1(1+\frac{1}{\kappa})\kappa}{n^{2/3}(E_1 + E_1\kappa - E_1\alpha\kappa)^{1/3}} \quad \text{(A17)}$$

$$\overline{\Delta T_2} = \frac{E_2}{n^{2/3}(E_1 + E_2 - E_2\alpha)^{1/3}} = \frac{E_1\kappa}{n^{2/3}(E_1 + E_1\kappa - E_1\alpha\kappa)^{1/3}} \quad \text{(A18)}$$

The characteristic equation of realization 2 can be easily obtained as follows:

$$\lambda^2 + \frac{n(5+(4-5\alpha)\kappa)\sqrt{\frac{(E_1(1+\kappa-\alpha\kappa))^{2/3}}{n^{2/3}}}\lambda}{2(1+\kappa-\alpha\kappa)} + \frac{3}{2}n^{4/3}(E_1(1+\kappa-\alpha\kappa))^{2/3} = 0 \quad \text{(A19)}$$

Given $\kappa = \frac{E_2}{E_1} > 0$, to ensure that a real solution exists for Eqs. (A17) and (A18), we have $E_1 + E_1\kappa - E_1\alpha\kappa > 0$, and we consider heat source in zone 2 is positive as well, we have $\kappa > 0$. Therefore, $\alpha < \frac{1+\kappa}{\kappa}$.

Assuming $\beta = \frac{n(5+(4-5\alpha)\kappa)\sqrt{\frac{(E_1(1+\kappa-\alpha\kappa))^{2/3}}{n^{2/3}}}}{2(1+\kappa-\alpha\kappa)}$, and $\gamma = \frac{3}{2}n^{4/3}(E_1(1+\kappa-\alpha\kappa))^{2/3}$.

The root of Eq.(A19) is the eigenvalue of matrix A_1. The eigenvalue is given as $\lambda_{1,2} = -\beta \pm \sqrt{\beta^2 - 4\gamma}$. Since $E_1(1+\kappa-\alpha\kappa) > 0$, and $n > 0$, thus $\gamma = \frac{3}{2}n^{4/3}(E_1(1+\kappa-\alpha\kappa))^{2/3} > 0$. Hence, $\lambda_{1,2}$ are determined by the real part of β. When $\beta > 0$, the real part of the eigenvalue is negative; otherwise, the real part of the eigenvalue is

positive. To ensure the solution of this differential equation is stable, the root of the characteristic equation should be less than zero. That is $-\beta = -\frac{n(5+(4-5\alpha)\kappa)\sqrt{\frac{(E_1(1+\kappa-\alpha\kappa))^{2/3}}{n^{2/3}}}\lambda}{2(1+\kappa-\alpha\kappa)} < 0$. Therefore, $5+(4-5\alpha)\kappa > 0$, that is $\alpha < \frac{5+4\kappa}{5\kappa}$.

In summary, when $\frac{5+4\kappa}{5\kappa} < \alpha < \frac{1+\kappa}{\kappa}$, the real parts of two eigenvalues are positive, the fixed point is unstable; when $\alpha < \frac{5+4\kappa}{5\kappa}$, the real parts of two eigenvalues are negative, the fixed point is stable; when $\frac{1+\kappa}{\kappa} < \alpha$, no fixed point exists.

Appendix B1 Dynamical analysis of Eqs.2-31 and 2-32

Denote the steady state solution(fixed point) of realization 1(Eqs.2-31 and 2-32) is $(\overline{\Delta T_1}, \overline{\Delta T_2})$, we can obtain:

$$\overline{\Delta T_1} = 0 \quad \text{(B1)}$$

$$\overline{\Delta T_2} = \frac{{E_1}^{2/3}}{n^{2/3}\alpha^{1/3}} \quad \text{(B2)}$$

After linearization of Eqs. 2-31 and 2-32 at the fixed point, the characteristic equation of realization 1 can be easily obtained as follows:

$$\lambda^2 + \frac{5n\sqrt{\alpha\overline{\Delta T_2}}\lambda}{2} + \frac{3}{2}n^2\alpha\overline{\Delta T_2} = 0 \quad \text{(B3)}$$

Assuming $\beta = \frac{5n\sqrt{\alpha\overline{\Delta T_2}}}{2}$, and $\gamma = \frac{3}{2}n^2\alpha\overline{\Delta T_2}$, by solving Eq.(B3), two eigenvalue of matrix A_1 are given as $\lambda_{1,2} = -\beta \pm \sqrt{\beta^2 - 4\gamma}$. Since $\alpha\overline{\Delta T_2} > 0$ and $n > 0$, hence, $\gamma = \frac{3}{2}n^2\alpha\overline{\Delta T_2} > 0$. Therefore, $\lambda_{1,2}$ are determined by the real part of β. Since $-\beta = -\frac{5n\sqrt{\alpha\overline{\Delta T_2}}}{2} < 0$ always holds, two eigenvalues are always negative, and a stable fixed point always exists for realization 1.

Appendix B2 Dynamical analysis of Eqs.2-33 and 2-34

Assuming the fixed point of realization 2(Eqs.2-33 and 2-34) is $\left(\overline{\Delta T_1},\ \overline{\Delta T_2}\right)$, we obtain:

$$\overline{\Delta T_1} = \frac{{E_1}^{2/3}}{n^{2/3}} \quad \text{(B4)}$$

$$\overline{\Delta T_2} = 0 \quad \text{(B5)}$$

After linearization of Eqs.2-33 and 2-34 at fixed point，the characteristic equation of realization 2 can be easily obtained as follows：

$$\lambda^2 + \frac{5n\sqrt{\overline{\Delta T_1}}\lambda}{2} + \frac{3}{2}n^2\overline{\Delta T_1} = 0 \quad \text{(B6)}$$

Assuming $\beta = \frac{5n\sqrt{\overline{\Delta T_1}}}{2}$, and $\gamma = \frac{3}{2}n^2\overline{\Delta T_1}$, by solving Eq.(B6), two eigenvalue of matrix A_1 are given as $\lambda_{1,2} = -\beta \pm \sqrt{\beta^2 - 4\gamma}$. Since $\overline{\Delta T_1} = \frac{{E_1}^{2/3}}{n^{2/3}} > 0$ and $n > 0$, thus $\gamma = \frac{3}{2}n^2\overline{\Delta T_1} > 0$. Therefore, $\lambda_{1,2}$ are determined by the real part of β. Since $-\beta = -\frac{5n\sqrt{\overline{\Delta T_1}}}{2} < 0$ always holds，two eigenvalues are always negative，and a stable fixed point always exists for realization 2.

Figure captions

Fig. 1. Schematics of a typical two-zone underground structure.

Fig. 2. Schematics of a typical two-zone underground structure with one local heat source.

Fig. 3. Modeled results validation: (a) Temperature comparison between the two zone model and previous CFD results; (b) Mass flow rates comparison between the two zone model and previous CFD results.(S1 indicates status1/realization 1, #-(1,2) indicates zone number)

Fig. 4. Bifurcation diagram for scenario1 ($\kappa = 1$): (a). Bifurcation diagram of mass flow rates; (b). Bifurcation diagram of temperature difference.

Fig. 5. Phase portrait and vector field for scenario 1: (a).Phase portrait and vector field for $\kappa = 1, \alpha = 0.4$; (b).Phase portrait and vector field for $\kappa = 1, \alpha = 0.54$;(c).Phase portrait and vector field

for $\kappa = 1, \alpha = 1.2$;(d).Phase portrait and vector field for $\kappa = 1, \alpha = 1.9$; (e).Phase portrait and vector field for $\kappa = 1, \alpha = 3$

Fig. 6. Bifurcation diagram for scenario 2($\alpha = 1$): (a). Bifurcation diagram of mass flow rates; (b). Bifurcation diagram of temperature difference.

Fig. 7. Phase portrait for scenario 2: (a).Phase portrait and vector field for $\kappa = -1, \alpha = 1$; (b).Phase portrait and vector field for $\kappa = 0.1, \alpha = 1$;(c).Phase portrait and vector field for $\kappa = 1, \alpha = 1$;(d).Phase portrait and vector field for $\kappa = 6, \alpha = 1$.

Fig. 8. Phase portrait and vector field for scenario 3(one local heat source at the bottom).

Fig. 9. Basic information of the hydro power station.

Fig. 10.Phase portrait and vector field for the dynamic system of buoyancy ventilation in the hydropower station.

Table captions

Table 1. Criterion for scenario 1

Table 2. Criterion for scenario 2

References

1. Mukhtar, A., K.C. Ng, and M.Z. Yusoff, *Design optimization for ventilation shafts of naturally-ventilated underground shelters for improvement of ventilation rate and thermal comfort.* Renewable Energy, 2018. **115**: p. 183-198. DOI: https://doi.org/10.1016/j.renene.2017.08.051.
2. Porras-Amores, C., et al., *Natural ventilation analysis in an underground construction: CFD simulation and experimental validation.* Tunnelling and Underground Space Technology, 2019. **90**: p. 162-173. DOI: https://doi.org/10.1016/j.tust.2019.04.023.
3. Liu, Z., et al., *On-site assessments on variations of PM2.5, PM10, CO2 and TVOC concentrations in naturally ventilated underground parking garages with traffic volume.* Environmental Pollution, 2019. **247**: p. 626-637. DOI: https://doi.org/10.1016/j.envpol.2019.01.095.
4. Zhao, Y., et al., *Seasonal patterns of PM10, PM2.5, and PM1.0 concentrations in a naturally ventilated residential underground garage.* Building and Environment, 2017. **124**: p. 294-314. DOI: https://doi.org/10.1016/j.buildenv.2017.08.014.

5. Cheng, L.H., T.H. Ueng, and C.W. Liu, *Simulation of ventilation and fire in the underground facilities.* Fire Safety Journal, 2001. **36**(6): p. 597-619. DOI: https://doi.org/10.1016/S0379-7112(01)00013-3.
6. Alkaff, S.A., S.C. Sim, and M.N. Ervina Efzan, *A review of underground building towards thermal energy efficiency and sustainable development.* Renewable and Sustainable Energy Reviews, 2016. **60**: p. 692-713. DOI: https://doi.org/10.1016/j.rser.2015.12.085.
7. Mukhtar, A., M.Z. Yusoff, and K.C. Ng, *The potential influence of building optimization and passive design strategies on natural ventilation systems in underground buildings: The state of the art.* Tunnelling and Underground Space Technology, 2019. **92**: p. 103065. DOI: https://doi.org/10.1016/j.tust.2019.103065.
8. Liu, Y., et al., *A network model for natural ventilation simulation in deep buried underground structures.* Building and Environment, 2019. **153**: p. 288-301. DOI: https://doi.org/10.1016/j.buildenv.2019.01.045
9. Li, A., X. Gao, and T. Ren, *Study on thermal pressure in a sloping underground tunnel under natural ventilation.* Energy and Buildings, 2017. **147**: p. 200-209. DOI: https://doi.org/10.1016/j.enbuild.2017.04.060.
10. Li, Y.Z. and H. Ingason, *Overview of research on fire safety in underground road and railway tunnels.* Tunnelling and Underground Space Technology, 2018. **81**: p. 568-589. DOI: https://doi.org/10.1016/j.tust.2018.08.013.
11. Li, M., S.M. Aminossadati, and C. Wu, *Numerical simulation of air ventilation in super-large underground developments.* Tunnelling and Underground Space Technology, 2016. **52**: p. 38-43. DOI: https://doi.org/10.1016/j.tust.2015.11.009
12. Batchelor, G., *Heat convection and buoyancy effects in fluids.* Quarterly journal of the royal meteorological society, 1954. **80**(345): p. 339-358. DOI: https://doi.org/10.1002/qj.49708034504
13. Khanal, R. and C. Lei, *Solar chimney—A passive strategy for natural ventilation.* Energy and Buildings, 2011. **43**(8): p. 1811-1819. DOI: https://doi.org/10.1016/j.enbuild.2011.03.035
14. Zhai, X.Q., Z.P. Song, and R.Z. Wang, *A review for the applications of solar chimneys in buildings.* Renewable and Sustainable Energy Reviews, 2011. **15**(8): p. 3757-3767. DOI: https://doi.org/10.1016/j.rser.2011.07.013
15. Zhou, J. and Y. Chen, *A review on applying ventilated double-skin facade to buildings in hot-summer and cold-winter zone in China.* Renewable and Sustainable Energy Reviews, 2010. **14**(4): p. 1321-1328. DOI: https://doi.org/10.1016/j.rser.2009.11.017
16. Shameri, M.A., et al., *Perspectives of double skin façade systems in buildings and energy saving.* Renewable and Sustainable Energy Reviews, 2011. **15**(3): p. 1468-1475. DOI: https://doi.org/10.1016/j.rser.2010.10.016
17. Saroglou, T., et al., *A study of different envelope scenarios towards low carbon high-rise buildings in the Mediterranean climate - can DSF be part of the solution?* Renewable and Sustainable Energy Reviews, 2019. **113**: p. 109237. DOI: https://doi.org/10.1016/j.rser.2019.06.044

18. Ghaffarianhoseini, A., et al., *Exploring the advantages and challenges of double-skin façades (DSFs).* Renewable and Sustainable Energy Reviews, 2016. **60**: p. 1052-1065. DOI: https://doi.org/10.1016/j.rser.2016.01.130
19. De Gracia, A., et al., *Numerical modelling of ventilated facades: A review.* Renewable and Sustainable Energy Reviews, 2013. **22**: p. 539-549. DOI: https://doi.org/10.1016/j.rser.2013.02.029
20. Barbosa, S. and K. Ip, *Perspectives of double skin façades for naturally ventilated buildings: A review.* Renewable and Sustainable Energy Reviews, 2014. **40**: p. 1019-1029. DOI: https://doi.org/10.1016/j.rser.2014.07.192
21. Stabat, P., M. Caciolo, and D. Marchio, *Progress on single-sided ventilation techniques for buildings.* Advances in Building Energy Research, 2012. **6**(2): p. 212-241. DOI: https://dx.doi.org/10.1080/17512549.2012.740903
22. Lo, L.J. and A. Novoselac. *Effect of indoor buoyancy flow on wind-driven cross ventilation*. in *Building Simulation*. 2013. Springer. DOI: https://doi.org/10.1007/s12273-012-0094-3
23. Stavridou, A.D. and P.E. Prinos, *Natural ventilation of buildings due to buoyancy assisted by wind: Investigating cross ventilation with computational and laboratory simulation.* Building and Environment, 2013. **66**: p. 104-119. DOI: https://doi.org/10.1016/j.buildenv.2013.04.011
24. Hunt, G. and P. Linden, *The fluid mechanics of natural ventilation—displacement ventilation by buoyancy-driven flows assisted by wind.* Building and Environment, 1999. **34**(6): p. 707-720. DOI: https://doi.org/10.1016/s0360-1323(98)00053-5
25. Nitta, K. *Variety modes and chaos in smoke ventilation by ceiling chamber system*. in *Proceedings of the Sixth International IBPSA Conference, Kyoto, Japan*. 1999.
26. Heiselberg, P., et al., *Experimental and CFD evidence of multiple solutions in a naturally ventilated building.* Indoor Air, 2004. **14**(1): p. 43-54. DOI: https://doi.org/10.1046/j.1600-0668.2003.00209.x
27. Li, Y. and A. Delsante, *Natural ventilation induced by combined wind and thermal forces.* Building and Environment, 2001. **36**(1): p. 59-71. DOI: https://doi.org/10.1016/s0360-1323(99)00070-0
28. Lishman, B. and A.W. Woods, *On transitions in natural ventilation flow driven by changes in the wind.* Building and Environment, 2009. **44**(4): p. 666-673. DOI: https://doi.org/10.1016/j.buildenv.2008.05.012
29. Li, Y., et al., *Some examples of solution multiplicity in natural ventilation.* Building and Environment, 2001. **36**(7): p. 851-858. DOI: https://doi.org/10.1016/s0360-1323(01)00011-7
30. Yuan, J. and L. Glicksman, *Multiple steady states in a combined buoyancy and wind driven natural ventilation system: necessary conditions and initial values.* Proceedings of indoor air, 2005: p. 1207-1212.
31. Yuan, J. and L.R. Glicksman, *Transitions between the multiple steady states in a natural ventilation system with combined buoyancy and wind driven flows.* Building and

Environment, 2007. **42**(10): p. 3500-3516. DOI: https://doi.org/10.1016/j.buildenv.2006.10.045

32. Yuan, J. and L.R. Glicksman, *Multiple steady states in combined buoyancy and wind driven natural ventilation: The conditions for multiple solutions and the critical point for initial conditions.* Building and Environment, 2008. **43**(1): p. 62-69. DOI: https://doi.org/10.1016/j.buildenv.2006.11.035

33. Gladstone, C. and A.W. Woods, *On buoyancy-driven natural ventilation of a room with a heated floor.* Journal of fluid mechanics, 2001. **441**: p. 293-314. DOI: https://doi.org/10.1017/s0022112001004876

34. Pulat, E. and H.A. Ersan, *Numerical simulation of turbulent airflow in a ventilated room: Inlet turbulence parameters and solution multiplicity.* Energy and Buildings, 2015. **93**: p. 227-235. DOI: https://doi.org/10.1016/j.enbuild.2015.01.067

35. Chenvidyakarn, T. and A. Woods, *Multiple steady states in stack ventilation.* Building and Environment, 2005. **40**(3): p. 399-410. DOI: https://doi.org/10.1016/j.buildenv.2004.06.020

36. Durrani, F., M.J. Cook, and J.J. McGuirk, *Evaluation of LES and RANS CFD modelling of multiple steady states in natural ventilation.* Building and Environment, 2015. **92**: p. 167-181. DOI: https://doi.org/10.1016/j.buildenv.2015.04.027

37. Chen, Z.D. and Y. Li, *Buoyancy-driven displacement natural ventilation in a single-zone building with three-level openings.* Building and Environment, 2002. **37**(3): p. 295-303. DOI: https://doi.org/10.1016/s0360-1323(01)00021-x

38. Gong, J. and Y. Li, *Solution multiplicity of smoke flows in a simple building.* Fire Safety Science, 2008. **9**: p. 895-906. DOI: https://doi.org/10.3801/iafss.fss.9-895

39. Gong, J. and Y. Li, *Smoke flow bifurcation due to opposing buoyancy in two horizontally connected compartments.* Fire Safety Journal, 2013. **59**: p. 62-75. DOI: https://doi.org/10.1016/j.firesaf.2013.03.014

40. Yang, D., et al., *Multiple patterns of heat and mass flow induced by the competition of forced longitudinal ventilation and stack effect in sloping tunnels.* International Journal of Thermal Sciences, 2019. **138**: p. 35-46. https://doi.org/10.1016/j.ijthermalsci.2018.12.018

41. Yang, L., et al., *Nonlinear Dynamic Aalysis of Natural Ventilation in a Two-Zone Building: Part B—CFD Simulations.* HVAC&R Research, 2006. **12**(2): p. 257-278. DOI: https://doi.org/10.1080/10789669.2006.10391178

42. Yang, L., P. Xu, and Y. Li, *Nonlinear dynamic analysis of natural ventilation in a two-zone building: Part A—Theoretical analysis.* HVAC&R Research, 2006. **12**(2): p. 231-255. DOI: https://doi.org/10.1080/10789669.2006.10391177

43. Li, Y., et al., *Flow bifurcation due to opposing buoyancy in two vertically connected open cavities.* International journal of heat and mass transfer, 2006. **49**(19-20): p. 3298-3312. DOI: https://doi.org/10.1016/j.ijheatmasstransfer.2006.03.016

44. Yang, D., et al., *Multiple steady states of fire smoke transport in a multi-branch tunnel: Theoretical and numerical studies.* Tunnelling and Underground Space Technology, 2017. **61**: p. 189-197. DOI: https://doi.org/10.1016/j.tust.2016.10.009

45. Liu, Y., et al., *The formation of multi-steady-states of buoyancy ventilation in underground building.* Tunnelling and Underground Space Technology, 2018. **82**: p. 613-626. DOI: https://doi.org/10.1016/j.tust.2018.09.008

46. Axley, J., *Multizone airflow modeling in buildings: History and theory.* HVAC&R Research, 2007. **13**(6): p. 907-928. DOI: https://doi.org/10.1080/10789669.2007.10391462